



## King's Research Portal

DOI:

[10.1021/acs.jmedchem.1c00375](https://doi.org/10.1021/acs.jmedchem.1c00375)

*Document Version*

Publisher's PDF, also known as Version of record

[Link to publication record in King's Research Portal](#)

*Citation for published version (APA):*

Lapointe, G., Skepper, C. K., Holder, L. M., Armstrong, D., Bellamacina, C., Blais, J., Bussiere, D., Bian, J., Cepura, C., Chan, H., Dean, C. R., De Pascale, G., Dhumale, B., Fisher, L. M., Fulsunder, M., Kantariya, B., Kim, J., King, S., Kossy, L., ... Rivkin, A. (2021). Discovery and Optimization of DNA Gyrase and Topoisomerase IV Inhibitors with Potent Activity against Fluoroquinolone-Resistant Gram-Positive Bacteria. *Journal of Medicinal Chemistry*, 64(9), 6329-6357. <https://doi.org/10.1021/acs.jmedchem.1c00375>

### **Citing this paper**

Please note that where the full-text provided on King's Research Portal is the Author Accepted Manuscript or Post-Print version this may differ from the final Published version. If citing, it is advised that you check and use the publisher's definitive version for pagination, volume/issue, and date of publication details. And where the final published version is provided on the Research Portal, if citing you are again advised to check the publisher's website for any subsequent corrections.

### **General rights**

Copyright and moral rights for the publications made accessible in the Research Portal are retained by the authors and/or other copyright owners and it is a condition of accessing publications that users recognize and abide by the legal requirements associated with these rights.

- Users may download and print one copy of any publication from the Research Portal for the purpose of private study or research.
- You may not further distribute the material or use it for any profit-making activity or commercial gain
- You may freely distribute the URL identifying the publication in the Research Portal

### **Take down policy**

If you believe that this document breaches copyright please contact [librarypure@kcl.ac.uk](mailto:librarypure@kcl.ac.uk) providing details, and we will remove access to the work immediately and investigate your claim.

# Discovery and Optimization of DNA Gyrase and Topoisomerase IV Inhibitors with Potent Activity against Fluoroquinolone-Resistant Gram-Positive Bacteria

Guillaume Lapointe,\* Colin K. Skepper,\* Lauren M. Holder, Duncan Armstrong, Cornelia Bellamacina, Johanne Blais, Dirksen Bussiere, Jianwei Bian, Cody Cepura, Helen Chan, Charles R. Dean, Gianfranco De Pascale, Bhavesh Dhumale, L. Mark Fisher, Mangesh Fulsunder, Bhavin Kantariya, Julie Kim, Sean King, Lauren Kossy, Upendra Kulkarni, Jay Lakshman, Jennifer A. Leeds, Xiaolan Ling, Anatoli Lvov, Sylvia Ma, Swapnil Malekar, David McKenney, Wosenu Mergo, Louis Metzger, Keshav Mhaske, Heinz E. Moser, Mina Mostafavi, Sunil Namballa, Jonas Noeske, Colin Osborne, Ashish Patel, Darshit Patel, Tushar Patel, Philippe Piechon, Valery Polyakov, Krunal Prajapati, Katherine R. Prosen, Folkert Reck, Daryl L. Richie, Mark R. Sanderson, Shailesh Satasia, Bhautik Savani, Jogitha Selvarajah, Vijay Sethuraman, Wei Shu, Kyuto Tashiro, Katherine V. Thompson, Krishniah Vaarla, Lakhan Vala, Dennis A. Veselkov, Jason Vo, Bhavesh Vora, Trixie Wagner, Laura Wedel, Sarah L. Williams, Satya Yendluri, Qin Yue, Aregahegn Yifru, Yong Zhang, and Alexey Rivkin



Cite This: *J. Med. Chem.* 2021, 64, 6329–6357



Read Online

ACCESS |



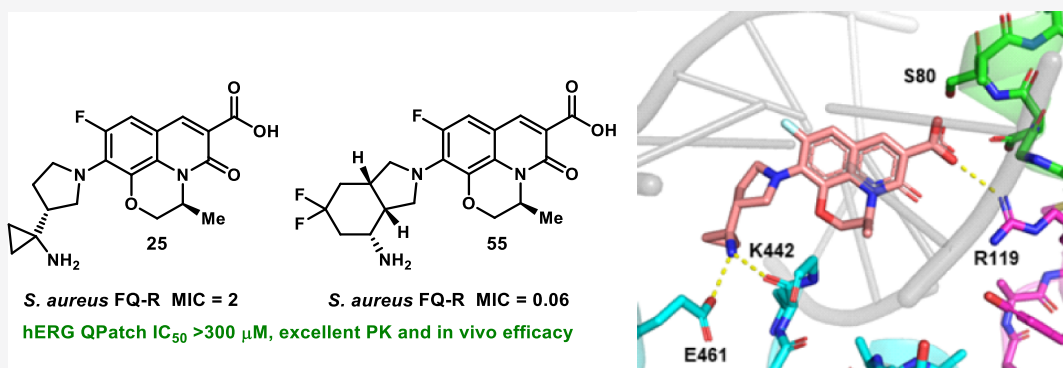
Metrics & More



Article Recommendations



Supporting Information



**ABSTRACT:** Herein, we describe the discovery and optimization of a novel series that inhibits bacterial DNA gyrase and topoisomerase IV *via* binding to, and stabilization of, DNA cleavage complexes. Optimization of this series led to the identification of compound **25**, which has potent activity against Gram-positive bacteria, a favorable *in vitro* safety profile, and excellent *in vivo* pharmacokinetic properties. Compound **25** was found to be efficacious against fluoroquinolone-sensitive *Staphylococcus aureus* infection in a mouse thigh model at lower doses than moxifloxacin. An X-ray crystal structure of the ternary complex formed by topoisomerase IV from *Klebsiella pneumoniae*, compound **25**, and cleaved DNA indicates that this compound does not engage in a water–metal ion bridge interaction and forms no direct contacts with residues in the quinolone resistance determining region (QRDR). This suggests a structural basis for the reduced impact of QRDR mutations on antibacterial activity of **25** compared to fluoroquinolones.

## INTRODUCTION

DNA gyrase and topoisomerase IV are structurally and functionally related targets of enormous importance for antibiotic chemotherapy. Both enzymes are essential for bacterial cell growth and are responsible for regulating the topology of bacterial DNA. Over the past 50 years, several

Received: March 2, 2021

Published: April 30, 2021



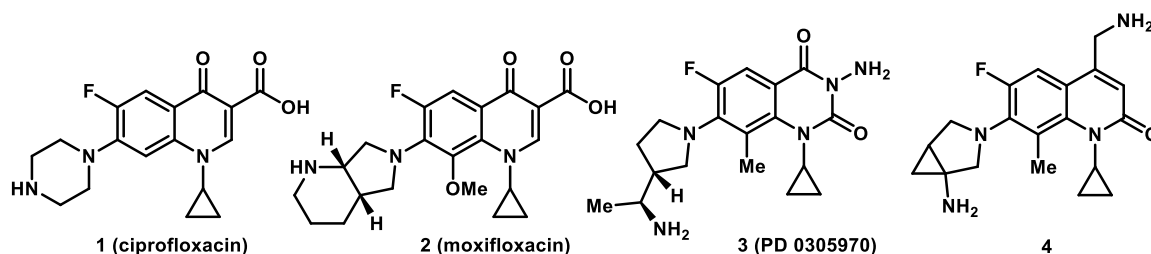


**Figure 1.** Structures of fluoroquinolone antibiotics ciprofloxacin (1) and moxifloxacin (2), quinazolidinedione PD 0305970 (3, Pfizer), and lead Gram-negative agent 4.

classes of inhibitors have been developed and advanced to either clinical trials or the market.<sup>1,2</sup> By far, the most medically and commercially successful of these are the quinolone antibiotics.<sup>3–9</sup> The first example of this class, nalidixic acid, can be traced to two parallel discovery efforts at Imperial Chemical Industries (ICI) and Sterling Drug during the late 1950s and early 1960s.<sup>10</sup> Since then, nearly 30 analogues have been approved for clinical use worldwide. One of the most widely used fluoroquinolones, ciprofloxacin (1, Figure 1), still accounts for over 20 million prescriptions annually in the US, despite having been in clinical use for three decades.<sup>11</sup>

As with all classes of antibiotics, bacterial resistance is a significant and growing problem that has already compromised the utility of quinolone antibiotics and threatens their future clinical use.<sup>12,13</sup> Quinolones act by binding to and stabilizing cleavage complexes formed between DNA gyrase or topoisomerase IV and substrate DNA. This results in inhibition of DNA replication and ultimately leads to chromosome fragmentation, induction of the SOS response, and rapid cell death.<sup>14,15</sup> A series of important biochemical and structural studies over the past several years have shed light on the precise mechanism by which quinolone antibiotics bind to and inhibit DNA gyrase and topoisomerase IV.<sup>16–19</sup> In particular, X-ray crystallography has illuminated a crucial interaction formed between the keto-acid motif of quinolones and a chelated  $Mg^{2+}$  cation. The metal cation in turn forms water-mediated hydrogen bonds with key residues in the GyrA and ParC subunits of DNA gyrase and topoisomerase IV, respectively. The amino acids involved in this interaction are generally serine (Ser80 in *Staphylococcus aureus* GrlA) and an acidic residue four positions downstream.<sup>20–23</sup> High-level resistance to quinolone antibiotics is usually driven by mutation of these residues in one or both of the target enzymes. These point mutations prevent formation of the crucial water–metal ion bridge interaction and render quinolones ineffective.<sup>12,13</sup> Due to the key role that they play in determining quinolone susceptibility, the portion of the enzyme in which these key residues reside is referred to as the quinolone resistance determining region (QRDR).<sup>24</sup>

Given the clinical importance of quinolone antibiotics, the discovery of DNA gyrase and topoisomerase IV inhibitors that can overcome quinolone resistance is an area of significant interest in antibacterial research.<sup>1,2,25</sup> Interest in this area was further bolstered by reports from Pfizer on a series of quinazolidinediones (e.g., compound 3, Figure 1) that are capable of binding to and stabilizing DNA gyrase/topoisomerase IV cleavage complexes but do not rely on formation of a water–metal ion bridge interaction.<sup>26–30</sup> To date, there have been no reports of compounds from this series reaching the clinic. More recently, researchers from the Innovative Medicines Initiative European Gram-negative Antibacterial

Engine (IMI-ENABLE) consortium reported the discovery of a series of imidazopyrazinones (IPYs) that also occupy the quinolone binding pocket without formation of the water–metal ion bridge.<sup>31,32</sup> As expected, both quinazolidinediones and IPYs showed minimal or no loss of susceptibility to strains that are resistant to fluoroquinolones.

As part of our broad efforts to discover new antibiotics for the treatment of resistant infections, we became interested in developing novel inhibitors of DNA gyrase and topoisomerase IV. To this end, we previously reported the discovery of a series of 4-(aminomethyl)quinolin-2(1H)-ones exemplified by compound 4 (Figure 1).<sup>33</sup> While structurally related to classical quinolone antibiotics, compounds such as 4 are devoid of both the C3 carboxylic acid and the C4 carbonyl that support the water–metal ion bridge important in quinolone binding. Nevertheless, extensive optimization yielded compounds with activity against relevant Gram-negative pathogens and minimal cross-resistance with quinolone antibiotics (e.g., ciprofloxacin). Unfortunately, insufficient potency and *in vitro* safety concerns ultimately led to the series being deprioritized.

In a related effort, we initiated an optimization campaign with the goal of identifying agents for the treatment of Gram-positive pathogens. Methicillin-resistant *S. aureus* (MRSA), drug-resistant *Streptococcus pneumoniae*, and vancomycin-resistant *Enterococcus*, for example, have all been identified by the Centers for Disease Control and Prevention (CDC) as serious threats to human health.<sup>34,35</sup> MRSA is recognized as a leading cause of healthcare-associated infections, and the CDC estimates that MRSA infections resulted in an estimated 10,600 deaths in 2017.<sup>35</sup> Recent surveys of methicillin- and oxacillin-resistant *S. aureus* clinical isolates indicate that roughly two-thirds are fluoroquinolone-resistant,<sup>36,37</sup> highlighting the need for new antibiotics in this area.

## RESULTS AND DISCUSSION

**Lead Series Optimization.** We began by profiling moxifloxacin (2) and compound 4 in addition to several analogues that were synthesized contemporaneously with that series (5–8, Table 1). Compounds 4–6 exhibited good antibacterial activity against both wild-type, fluoroquinolone-sensitive (WT, FQ-S), and fluoroquinolone-resistant (FQ-R) *S. aureus*. The latter strain is characterized by QRDR mutations in both DNA gyrase and topoisomerase IV, a combination that confers significant resistance to fluoroquinolone antibiotics. This is exemplified by a 64-fold decrease in potency for moxifloxacin (2) compared to the WT (FQ-S) strain. The potency exhibited by compounds 4–6 against this strain of FQ-R *S. aureus* was therefore deemed encouraging. However, all three compounds were compromised by hERG inhibition and cytotoxicity profiles that were inferior to moxifloxacin (2). In contrast, compound 7 was potent against FQ-S *S. aureus* but

Table 1. *In Vitro* Profile of Moxifloxacin (2) and Lead Compounds 5–8

	compounds						
	2	4	5	6	7	(±)-8	(-)-8
<i>S. aureus</i> FQ-S MIC ( $\mu\text{g/mL}$ )	0.06		$\leq 0.06$		0.125	0.06	0.06
<i>S. aureus</i> FQ-R MIC ( $\mu\text{g/mL}$ ) <sup>a</sup>	4	0.125	0.06	0.5	2	1	1
MIC fold shift (FQ-R/FQ-S)	64		$\geq 1$		16	16	16
$\log D_{7,4}$	0.63	1.1	0.74	0.32	-1.7	-0.97	-0.34
$\text{pK}_a$ <sup>b</sup>	9.1, 6.7	8.0, 7.6	9.6	10, 8.2	9.3, 5.2	8.6, 5.2	8.6, 5.1
cytotoxicity $\text{EC}_{50}$ HepG2, K562 ( $\mu\text{M}$ )	>100	82, 40	93, 49	74, 65	>100	>100	>100
hERG QPatch $\text{IC}_{50}$ ( $\mu\text{M}$ )	129 <sup>c</sup>	114 <sup>d</sup>	49 <sup>e</sup>	25 <sup>f</sup>	214 <sup>f</sup>	109 <sup>f</sup>	136 <sup>f</sup>

<sup>a</sup>GyrA (S84L); GrlA (S80F); GrlB (E471K). <sup>b</sup>Determined using the UV metric method (see the Experimental Section for details). <sup>c</sup>Literature value.<sup>38</sup> <sup>d</sup>Determined using QPatch automated electrophysiology with a long incubation protocol.<sup>33</sup> <sup>e</sup>Determined using manual patch clamp electrophysiology.<sup>33</sup> <sup>f</sup>Determined using QPatch automated electrophysiology (see the Experimental Section for details).

exhibited a moderate shift in the MIC value against the FQ-R strain (16-fold for 7 compared to 64-fold for moxifloxacin, 2). This feature was offset by positive attributes such as reduced  $\log D$ , cytotoxicity, and hERG inhibition compared to 4–6. A small potency boost was subsequently achieved, without compromising *in vitro* safety parameters, upon introduction of a modified C7 amine (8). We observed that racemic and enantiopure amines provided compounds with nearly identical properties (*i.e.*, (±)-8 and (-)-8).

With the goal of developing a candidate for use against quinolone-resistant Gram-positive infections, we chose to prioritize *in vitro* safety and thus (-)-8 became our starting point for further optimization. Our medicinal chemistry strategy was guided, in large part, by the requirement for both an excellent safety profile and low efficacious dose to support potential administration of any new drug in the outpatient setting. For example, while compound 8 is not a potent hERG channel inhibitor ( $\text{IC}_{50} = 109\text{--}136 \mu\text{M}$ ), further improvements were required in order to maintain a window of  $\geq 30$ -fold over the anticipated efficacious plasma free drug concentration ( $\sim 5\text{--}10 \mu\text{M}$  based upon data from quinolone antibiotics).<sup>39</sup> Moxifloxacin (2) provided a useful point of comparison; with similar levels of *in vitro* hERG inhibition to (-)-8,<sup>38</sup> 2 has been reported to induce QT prolongation in humans at therapeutic doses.<sup>40,41</sup>

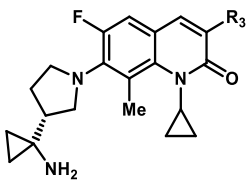
As can be seen from the data in Table 1, compound (-)-8 displayed a 16-fold shift in MIC between WT and FQ-R strains of *S. aureus*. While this was a modest improvement over moxifloxacin (64-fold), we were interested in further exploring the SAR at the C3 position to either reduce the impact of QRDR mutations on MIC, improve intrinsic potency, or both. This was also attractive from a scientific standpoint, given the paucity of SAR at the corresponding position on the classical quinolone scaffold.

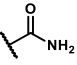
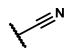
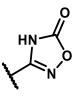
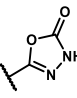
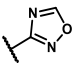
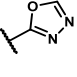
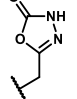
Data generated from early analogues suggested that a polar and possibly ionizable group at C3 was preferred from an *in vitro* safety perspective. Replacement of the C3 carboxylic acid in (-)-8 with neutral, polar groups such as a primary amide or nitrile (9 and 10, respectively) provided compounds with potent activity against WT *S. aureus* and minimal MIC shift

against the FQ-R strain (Table 2). Unfortunately, both compounds proved to be potent hERG binders, and thus, our focus turned to ionizable groups at this position, including a variety of weak carboxylic acid isosteres. Two notable examples included 11 and 12, which provided potent antibacterial activity against both WT and FQ-R *S. aureus*. This was interesting in light of the fact that both compounds possessed an acidic functional group with the potential for interaction with QRDR residues in DNA gyrase and topoisomerase IV. The oxadiazolone moiety of compound 11 exhibited a  $\text{pK}_a$  (5.4) that was very close to that measured for the carboxylic acid of (-)-8 (5.1). The isomeric oxadiazolone moiety of compound 12 was less acidic ( $\text{pK}_a = 7.2$ ). Unfortunately, both 11 and 12 proved to be relatively potent hERG binders. The neutral heterocycles 13 and 14 had excellent antibacterial activity but with a clear hERG inhibition liability. Compounds 9–14 provide unique insights into the spectrum of functional groups tolerated at this position of the quinolone scaffold from a relatively small nitrile (10) to more bulky heterocycles (11–14). However, the limits of the binding pocket were realized upon synthesis of 15, which extends the heterocycle of 12 by a single methylene, which proved deleterious to antibacterial activity.

With these results in hand, we moved to examine the SAR at the C4 position in the hopes of identifying potent compounds with an improved *in vitro* safety profile. Several acidic heterocycles were screened with direct attachment to the C4 position, providing 16–18 (Table 3). These compounds were less potent than their C3-substituted counterparts, and hERG binding was not improved. We were pleased to find, however, that by inserting a methylene spacer between the heterocycle and the core, we were able to generate compounds with reduced hERG binding ( $\text{IC}_{50} > 30 \mu\text{M}$ ) that maintained reasonable antibacterial activity (19–22). This small series of analogues featured  $\text{pK}_a$  values for the acidic moiety ranging from 2.5 (20) to 7.2 (22) with the latter proving optimal for antibacterial activity. In addition, a number of analogues with neutral substituents at C4 were examined, including dimethyl amide 23. While larger alkyl substituents were tolerated on the amide nitrogen, none provided any benefit in terms of

Table 2. Survey of SAR at the C3 Position of Compound 8



Cmpds	R <sub>3</sub>	MIC (μg/mL)			pK <sub>a</sub> <sup>c</sup>	hERG binding IC <sub>50</sub> (μM) <sup>d</sup>
		<i>S. aureus</i> FQ-S	<i>S. aureus</i> FQ-R <sup>a</sup>	log D <sub>7.4</sub>		
9		0.25	1	-	8.4	10
10 <sup>b</sup>		0.06	0.06	1.19	8.4	2.7
11		0.125	0.125	-0.32	8.5, 5.4	29
12		0.125	0.06	-	8.5, 7.2	10
13 <sup>b</sup>		0.25	0.5	1.46	8.4	12
14		0.125	0.125	-	8.3	8
15		32	32	0.87	8.8	-

<sup>a</sup>GyrA (S84L); GrlA (S80F); GrlB (E471K). <sup>b</sup>Compound was prepared using racemic C7 amine. <sup>c</sup>Determined using the UV metric method (see the Experimental Section for details). <sup>d</sup>Determined by hERG radioligand displacement assay with [<sup>3</sup>H]dofetilide (see the Experimental Section for details).

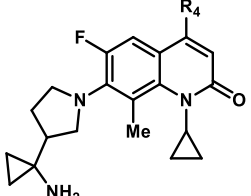
antibacterial activity (data not shown). Compound **23** was found to exhibit an *in vitro* profile very similar to that seen for **22**; indeed, from the compounds presented in Table 3, **22** and **23** provided the best overall balance of antibacterial activity and *in vitro* safety. Both compounds were subsequently advanced to *in vivo* pharmacokinetic (PK) experiments and further *in vitro* safety profiling.

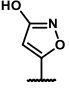
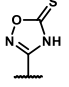
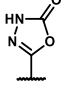
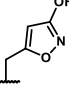
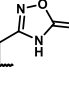
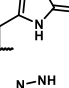
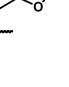
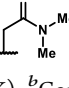
We were pleased to find that compounds **22** and **23** showed reduced hERG inhibition relative to (±)-**8**, with moderate levels of plasma protein binding (PPB, Table 4). Unfortunately, both **22** and **23** suffered from moderately high *in vivo* clearance, relatively low exposure, and poor oral bioavailability in rats. This profile was representative of compounds in this series, and our attempts to identify analogues with improved PK were not successful. In contrast, (±)-**8** possessed an excellent PK profile, which prompted us to re-examine our strategy of replacing the C3 carboxylic acid. Although compounds which lacked the C3 carboxylic acid were often potent against both WT and FQ-R Gram-positive bacteria, it proved challenging to balance this activity with adequate *in vitro* safety and/or PK properties.

Returning to **8** as a starting point for optimization, two major liabilities needed to be addressed: hERG inhibition and plasma protein binding. With respect to plasma protein

binding, we anticipated that values in the range of 70–80% bound drug would make it challenging to achieve efficacious free plasma exposure with reasonable doses. It thus became a priority to identify compounds with reduced plasma protein binding that did not sacrifice the otherwise good PK profile of compound **8** and further improved upon the hERG inhibition profile. We found limited success in addressing these parameters in the context of the core scaffold present in **8**, and this prompted us to examine alternate cores. A number of candidates were profiled, among them, compounds **24** and **25**. Both featured a tricyclic core that was adapted from levofloxacin, a fluoroquinolone which is widely recognized as having a favorable safety profile and has found much clinical success.<sup>42</sup> This scaffold morphing approach yielded compounds with an excellent *in vitro* and *in vivo* profile (Table 5). Antibacterial potency for **24** and **25** was very similar to (–)-**8**, with all three compounds exhibiting a spectrum of activity that included coverage of *S. aureus*, *S. pneumoniae*, and *Enterococcus faecalis*. For both matched pairs (*i.e.*, **7** and **24**, (–)-**8** and **25**) the tricyclic core afforded a remarkable improvement in terms of hERG inhibition, PPB, and solubility. Further profiling of **24** and **25** revealed no liabilities with respect to sodium or calcium channel inhibition. Cytotoxicity was assessed against HepG2

Table 3. Survey of SAR at the C4 Position of Compound 8



Cmpds	MIC (μg/mL)		log <i>D</i> <sub>7.4</sub>	p <i>K</i> <sub>a</sub> <sup>c</sup>	hERG binding IC <sub>50</sub> (μM) <sup>e</sup>	
	<i>S. aureus</i> FQ-S	<i>S. aureus</i> FQ-R <sup>d</sup>				
16 <sup>b</sup>		1	2	0.29	8.6, 4.7	17
17		4	4	-	8.7, 2	18
18		0.5	1	-	8.6, 6.4	13
19		8	8	-0.9	8.5, 3.9	>30
20		8	8	-0.3	8.6, 2.5	>30
21		4	32	-0.74	8.5, 5.1	>30
22		1	0.5	0.24	8.4, 7.2 <sup>d</sup>	>30
23		2	1	0.27	8.5	>30

<sup>a</sup>GyrA (S84L); GrlA (S80F); GrlB (E471K). <sup>b</sup>Compound was prepared using enantiopure C7 amine. <sup>c</sup>Determined using UV metric method (see Experimental Section). <sup>d</sup>Determined using solution potentiometry method (see Experimental Section). <sup>e</sup>Determined by hERG radioligand displacement assay with [<sup>3</sup>H]dofetilide (see Experimental Section for details).

and K562 cell lines, and the EC<sub>50</sub> of both **24** and **25** exceeded 100 μM.

With these data in hand, the tricyclic scaffold exemplified by **24** and **25** became the lead series, and we moved rapidly to explore the SAR at all available positions with the primary goal of improving antibacterial activity. We began by making modifications to the morpholine ring embedded in the structure of **25**. Inverting the methyl branch stereocenter led to significant loss of potency (**26**, Table 6) while expanding to a seven-membered ring was better tolerated but did not offer any apparent benefit (**27**). Replacing the ether oxygen with a methylene led to compound **28**, which was twofold more potent than the parent compound but was somewhat more lipophilic with slightly increased hERG inhibition. Truncating this embedded ring to a five-membered heterocycle provided **29**, which displayed antibacterial activity similar to **27**. Further substitution on the methyl branch was not well tolerated (data

not shown), thus establishing the core structure of **25** as optimal.

Exploration of the SAR at C5 and C6 uncovered several interesting trends. We found that addition of a fluorine or chlorine at C5 (**30** and **31**, respectively) led to an increase in potency that tracked with a gradual increase in log *D* but was accompanied by an increase in hERG inhibition (Table 7). Polar groups at C5 were also tolerated (**32** and **33**) but offered no significant improvement over **25**. Removing the prototypical C6 fluorine (which is nearly ubiquitous in modern quinolone antibiotics) from **25** provided **34**. This simple modification was tolerated in terms of antibacterial activity but had a surprising effect on hERG inhibition (IC<sub>50</sub> = 90 μM for **34** vs >300 μM for **25**). Introducing a single fluorine or chlorine at C5 provided compounds with slightly improved potency but led to a surprisingly large increase in hERG inhibition (**35** and **36**). Nitrile analogues **37** and **38** offered a

**Table 4. hERG Inhibition Data, Plasma Protein Binding, and PK of 22, 23, and (±)-8 in Rats<sup>a</sup>**

	22	23	(±)-8
hERG QPatch IC <sub>50</sub> (μM)	188	293	109
PPB % bound (m/r/h)	60/85/73	42/67/43	52/75/78
CL (mL/min·kg)	46.2	49.3	7.05
V <sub>ss</sub> (L/kg)	1.3	3.3	0.69
t <sub>1/2term. iv</sub> (h)	0.99	1.61	1.32
AUC <sub>inf</sub> (μM·h)/dose (mg/kg) iv	0.82	0.80	6.24
AUC <sub>inf</sub> (μM·h)/dose (mg/kg) po	0.12	0.26	7.62
C <sub>max</sub> (μM)/dose (mg/kg) po	0.051	0.078	2.0
T <sub>max</sub> po (h)	0.5	1.17	1.0
oral BA (% F)	14.9	32.5	Quantitative

<sup>a</sup>All compounds were administered as solutions of the corresponding hydrochloride salt. Dose = 2.5 mg/kg (IV) and 5 mg/kg (PO). Vehicle = 20% PEG300 + 5% Solutol in D5W.

profile similar to **25** but without sufficient differentiation to warrant further follow-up. Replacing the C6 fluorine with chlorine or methoxy (**39** and **40**) was poorly tolerated in terms of antibacterial activity.

Of all the positions on the classical quinolone scaffold, C7 has historically been most amenable to modification. This is clearly reflected by the enormous number of analogues that have been synthesized and reported in the primary and patent literature.<sup>43</sup> We surveyed this position broadly in the context of compound **25**, and a selection of analogues is presented in Table 8. We found that, in general, antibacterial activity was optimal with analogues that retained the 3-(aminomethyl)pyrrolidine substructure found in **24** and **25**. Subtle changes, such as expanding the cyclopropylamine of **25** to give cyclobutylamine **41** were tolerated, as was additional substitution at the C4 position of the pyrrolidine ring (e.g., **42**). Amine moieties derived from fluoroquinolones either on

the market or reported in the literature often displayed moderate to poor antibacterial activity (**43–45**).<sup>44</sup> Analogues which featured a C7 pyrrolidine with a heteroatom directly attached were poorly active, particularly against FQ-R *S. aureus* (**46** and **47**).

A significant boost in potency was realized with the cis-fused bicyclic amine of **48** (Table 9). This resulted in eight-fold improved activity against FQ-R *S. aureus* relative to **25**. This particular bicyclic amine, along with a series of related structures, has found use previously as C7 substituents in antibacterial fluoroquinolones.<sup>45,46</sup> Up to this point, the most potent C7 moiety had been that associated with compound **24**. Accumulated SAR suggested that correct placement of the basic amine was important for antibacterial activity, and it may be that **48** derived additional potency through conformational restriction of the C7 moiety. Comparison of small-molecule crystal structures of **24** and **48** showed the basic amine occupying nearly identical positions for the two compounds (see Figure S11). The other three possible stereoisomers of **48** (featuring a cis-fused junction between the 5- and 6-membered rings) were prepared, but all were less potent than **48** (data not shown). Interestingly, trans-fused bicyclic amine **49** was nearly equipotent to **48**. Overlay of the corresponding small molecule X-ray crystal structures revealed nearly identical placement of the basic amine in **48** and **49** (see Figure S12). Similar to **48**, the other other possible stereoisomers of **49** with a trans-fused ring junction were markedly less potent (data not shown).

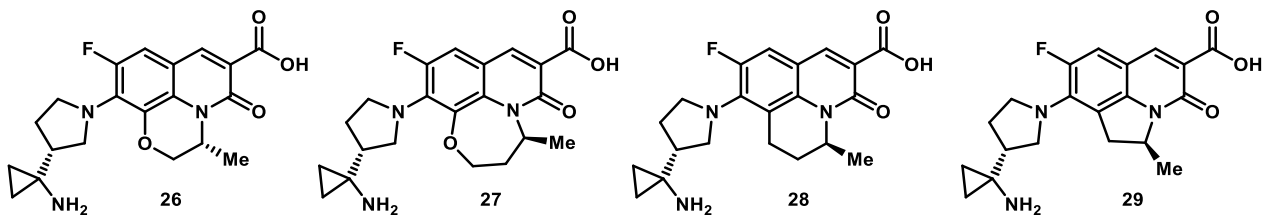
The added lipophilicity and higher amine pK<sub>a</sub> associated with **48**, however, lead to a significant increase in hERG inhibition (hERG QPatch IC<sub>50</sub> = 127 μM, assessed using a long incubation protocol<sup>47</sup>). Assessment of **49** in the QPatch assay indicated an IC<sub>50</sub> > 300 μM; however, the dose–response curve from this experiment suggested possible solubility issues at the upper concentration points. In order to reduce lipophilicity, the corresponding cyclic ethers **50** and **51** were prepared. These compounds were characterized by

**Table 5. In Vitro Profile of 5, 7, (–)-8, 24, and 25**

	5	7	(–)-8	24	25
<i>S. aureus</i> FQ-S MIC (μg/mL)	≤0.06	≤0.06	0.06	0.125	0.25
<i>S. aureus</i> FQ-R MIC (μg/mL) <sup>a</sup>	0.06	2	1	2	2
<i>S. aureus</i> FQ-R clinical isolate MIC (μg/mL)	≤0.03	2	0.5	1	0.5
<i>E. faecalis</i> FQ-S MIC (μg/mL)	0.125	0.25	0.25	0.25	0.5
<i>S. pneumoniae</i> FQ-S MIC (μg/mL)	≤0.03	0.015	≤0.03	≤0.03	0.06
log D <sub>7.4</sub>	0.74	–1.7	–0.34	–1.1	–0.90
pK <sub>a</sub> <sup>b</sup>	9.6	9.3, 5.2	8.6, 5.1	9.6, 5.0	8.6, 4.9
solubility (PBS, μg/mL)	498	161	623	675	1268
Caco-2 (A–B, ER)	16.7 (1.5)	2.51 (7.5)	23.1 (0.91)	2.70 (1.7)	20.0 (0.90)
PPB (% bound m/r/h)	81/75/90	34/46/46	51/70/79	6/28/20	13/37/24
hERG QPatch IC <sub>50</sub> (μM) (% inh.@300 μM) <sup>c</sup>	49 <sup>d</sup>	181	136	>300 (8.3)	>300 (27)
Na <sub>v</sub> 1.5, Ca <sub>v</sub> 1.2 IC <sub>50</sub> (μM)	>50, NT	>50, NT	92, >500	>500, >500	>500, >500
cytotoxicity EC <sub>50</sub> HepG2, K562 (μM)	93, 49	>100, >100	>100, >100	>100, >100	>100, >100

<sup>a</sup>GyrA (S84L); GrlA (S80F); GrlB (E471K). <sup>b</sup>Determined using the UV-metric method (see the Experimental Section). <sup>c</sup>Determined using QPatch automated electrophysiology except for compound **5** (see the Experimental Section for details). <sup>d</sup>Determined using manual patch clamp electrophysiology.<sup>33</sup>

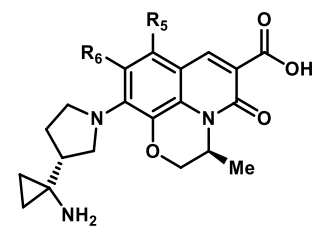
Table 6. SAR Exploration of the Central Morpholine Ring of 25



cmpds	MIC ( $\mu\text{g/mL}$ )		$\log D_{7.4}$	hERG QPatch IC <sub>50</sub> ( $\mu\text{M}$ ) <sup>b</sup>
	<i>S. aureus</i> FQ-S	<i>S. aureus</i> FQ-R <sup>a</sup>		
25	0.25	2	-0.90	>300
26	16	>32	-0.92	NT
27	0.25	8	0.01	>30 <sup>c</sup>
28	0.06	1	-0.27	297
29	0.25	8	-0.51	>30 <sup>c</sup>

<sup>a</sup>GyrA (S84L); GrlA (S80F); GrlB (E471K). <sup>b</sup>Determined using QPatch automated electrophysiology (see the Experimental Section for details). <sup>c</sup>Measured up to 30  $\mu\text{M}$ .

Table 7. Survey of SAR at the C5 and C6 Positions of the Compound 25 Scaffold



cmpds	MIC ( $\mu\text{g/mL}$ )		$\log D_{7.4}$	hERG QPatch IC <sub>50</sub> ( $\mu\text{M}$ ) <sup>b</sup>		
	R5	R6			<i>S. aureus</i> FQ-S	<i>S. aureus</i> FQ-R <sup>a</sup>
25	H	F	0.25	2	-0.90	>300
30	F	F	0.06	1	-0.85	211
31	Cl	F	$\leq 0.03$	0.5	-0.46	150
32	NH <sub>2</sub>	F	0.5	8	-0.97	NT
33	CN	F	0.125	1	-1.86	>30 <sup>c</sup>
34	H	H	0.25	4	-0.69	90
35	F	H	0.25	2	-0.40	126
36	Cl	H	0.125	1	0.46	42
37	CN	H	0.25	2	-0.55	>300
38	H	CN	0.25	4	-1.77	NT
39	H	Cl	2	32	-1.12	NT
40	H	OMe	32	>32	-1.22	NT

<sup>a</sup>GyrA (S84L); GrlA (S80F); GrlB (E471K). <sup>b</sup>Determined using QPatch automated electrophysiology (see the Experimental Section for details). <sup>c</sup>Measured up to 30  $\mu\text{M}$ .

lower  $\log D_{7.4}$  and reduced basicity relative to the parent analogues 48 and 49, and this translated into reduced hERG inhibition. Unfortunately, both compounds suffered from a 2–4 fold loss of antibacterial potency. Returning to the carbocyclic structure of 48, introduction of polar and electron-withdrawing substituents at the  $\gamma$ -position relative to the basic amine drove similar reductions in hERG inhibition (52–55). Assessment of 52 in the hERG QPatch assay indicated possible solubility issues at higher concentrations (similar to 49), although the IC<sub>50</sub> was judged to be >300  $\mu\text{M}$ . Difluoromethyl ether 53 provided a similar reduction in hERG inhibition but was found to be 4-fold less potent than 48 against FQ-R *S. aureus*. A single fluorine atom (compound 54) was subsequently found to be sufficient to drive a simultaneous

reduction in hERG inhibition and an increase in antibacterial potency. The gem-difluorinated derivative 55 provided a similarly excellent *in vitro* profile, accompanied by a further reduction in amine pK<sub>a</sub> as expected (measured pK<sub>a</sub> 48/54/55: 9.8 → 8.9 → 8.1). Substitution at the  $\delta$ -position (relative to the basic amine) with polar and electron-withdrawing groups also provided potent compounds with negligible hERG inhibition (e.g., compounds 56 and 57).

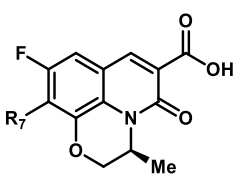
**Structural Characterization of the Binding Mode of 25 to *Klebsiella pneumoniae* Topoisomerase IV.** We previously described the use of a crystallization system based on a ParE–ParC fusion protein from *Klebsiella pneumoniae*.<sup>19</sup> This system yielded cocrystal structures with several small molecule ligands from the quinolin-2(1H)-one series including compound 4.<sup>33</sup> With the identification of the tricyclic series exemplified by 25, which unlike 4 features a C3 carboxylic acid, it became a priority to understand how the binding mode of such compounds compared to classical fluoroquinolone antibiotics.

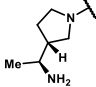
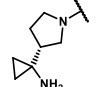
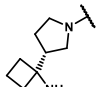
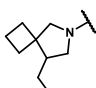
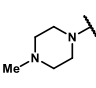
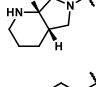
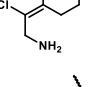
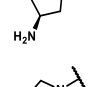
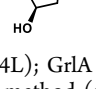
Toward this end, the ternary complex formed between the ParE–ParC fusion protein, DNA, and compound 25 provided crystals that diffracted to 3.3 Å (Figure 2 and Table S1). A symmetric 26bp duplex DNA, doubly nicked at the DNA cleavage site and lacking the 5'-phosphates, was used. Similar to the structure obtained previously with compound 4, the asymmetric unit contained two copies of the ParE–ParC fusion protein dimer. Each copy of the fusion protein dimer was bound to one doubly nicked DNA duplex, providing two sites for ligand binding. Unbiased electron density was observed for 25 in all four compound binding sites in the asymmetric unit (see Figure S1). Small differences in binding pose and electron density were observed between the four binding sites. The observations described below correspond to the binding site, which provided the best electron density.

As expected, compound 25 intercalates between adjacent base pairs at the DNA cleavage site and engages in  $\pi$ – $\pi$  stacking interactions with the DNA bases (see Figures 2A,B and S2). The basic amine of compound 25 forms interactions with the side chain of E461 and the backbone carbonyl of K442 located in the ParE subunit of the fusion protein. It should be noted that different orientations for the C7 pyrrolidine substituent were observed for compound 25 bound to the other copies of the cleavage site in the



Table 8. Survey of SAR at the C7 Position of the Compound 25 Scaffold



Cmpds	MIC (μg/mL)		log $D_{7.4}$	$pK_a^b$	
	<i>S. aureus</i> FQ-S	<i>S. aureus</i> FQ-R <sup>a</sup>			
24		0.125	2	-1.1	9.6, 5
25		0.25	2	-0.90	8.6, 4.9
41		0.125	2	-1.42	9.5, 4.9
42		0.125	2	-0.66	9.8, 5.2
43		16	>32	-1.99	8.3, 4.5
44		1	32	-1.46	9.7, 5
45		4	>32	-0.39	NT
46		2	>32	<-2.00	9.2, 4.8
47		0.5	>32	-0.46	5.2

<sup>a</sup>GyrA (S84L); GrlA (S80F); GrlB (E471K). <sup>b</sup>Determined using the UV metric method (see the Experimental Section).

asymmetric unit. In one other case, the interactions between the basic amine of 25 and the side chain of E461 and the backbone carbonyl of K442 were conserved, whereas in the other two cases, the interactions were lost. The C3 carboxylate is poised to form an interaction with the side chain of R119, albeit at a relatively long distance (3.2 Å). Electron density for the R119 side chain was only observed in one of the four compound binding sites, suggesting that this interaction may not contribute significantly to binding affinity.

The crystal structure of levofloxacin bound to topoisomerase IV from *K. pneumoniae* provides an instructive comparison.<sup>19</sup> While levofloxacin chelates a Mg<sup>2+</sup> cation that in turn forms water-mediated interactions with E84, no metal ion chelation is observed for compound 25. The core of compound 25 is also shifted significantly away from E84, with no direct interactions to either S80, E84, or surrounding residues in the QRDR

region (see Figure 2C). This may provide a structural basis for the reduced impact of QRDR mutations on the antibacterial activity of compound 25. Sequence comparison between ParE and ParC from *K. pneumoniae*, *S. aureus*, *E. faecalis*, and *S. pneumoniae* shows that the key residues highlighted in Figure 2 are well conserved between species (see Figure S3). This suggests that inferences made from the structure obtained with Gram-negative *K. pneumoniae* topoisomerase IV may also be relevant to the complex formed with the enzyme in common Gram-positive pathogens.

**In Vivo Profiling.** The low *in vitro* clearance, high permeability, and good solubility associated with compound 25 (see Table 5) translated to favorable PK properties in preclinical species (Table 10). Compound 25 exhibited low *in vivo* clearance and high bioavailability in mouse, rat, and dog; dose-normalized exposure was high and was observed to increase in the order dog > rat > mouse. By comparison, (–)-8 demonstrated good PK in rats although both IV and oral exposures were somewhat lower than 25. Compound 24, which differs from 25 only in the nature of the C7 amine, had significantly lower exposure in rats likely as a result of increased clearance. Compound 55, on the other hand, displayed a rat PK profile which was very similar to 25, with excellent oral bioavailability.

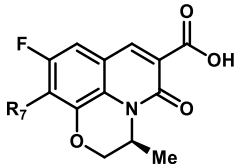
When combined with low plasma protein binding, the excellent PK properties of 25 translated to very high free plasma exposures. This in turn drove remarkable *in vivo* efficacy for compound 25, as demonstrated in the neutropenic murine thigh infection model when administered subcutaneously (Table 11). Against FQ-S *S. aureus* infection in mice, 25 was efficacious at lower doses than (–)-8, 55 or moxifloxacin, despite the fact that the latter three compounds are at least 4- to 8-fold more potent *in vitro* than 25. Compound 25 also achieved efficacy against infections caused by a FQ-R *S. aureus* clinical isolate at doses that were substantially lower than that observed with 24, which again was 2-fold more potent than 25 *in vitro*.

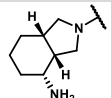
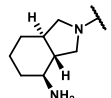
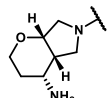
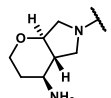
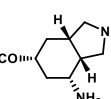
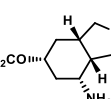
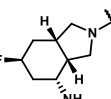
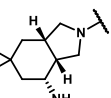
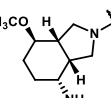
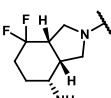
**Chemistry.** Compounds 5 and 7 were prepared according to procedures described previously.<sup>33</sup> The synthesis of 6 commenced with known intermediate 58, which was condensed with 2-methoxyethyl acetate, followed by cyclization to furnish 59 (Scheme 1). Buchwald–Hartwig coupling<sup>48–51</sup> with pyrrolidine 60 gave 61, which was globally deprotected using BBr<sub>3</sub> to afford 6.

Analogues of 6 featuring variations at the quinolone C3 position were prepared from the key bromide intermediate 62 (Scheme 2).<sup>33</sup> Buchwald–Hartwig coupling<sup>52,53</sup> with 63 provided 64 in good yield, which was subjected to ester hydrolysis and Boc deprotection, thus establishing a scalable route to compound 8. Intermediate acid 65 could also be converted to the primary amide 9 using conventional methods. Alternatively, coupling of 65 with formic hydrazide followed by cyclodehydration mediated by *p*-toluenesulfonyl chloride and Et<sub>3</sub>N yielded the corresponding 1,2,4-oxadiazole 14 in excellent yield following deprotection with trifluoroacetic acid (TFA).<sup>54</sup> The oxadiazolone 12 was accessed *via* formation of the C3 acylhydrazide (66), cyclization with triphosgene, and Boc deprotection with HCl in dioxane.

Several C3-analogues such as 10, 11, and 13 were accessed from a common C3 nitrile intermediate (69) as shown in Scheme 3. Conversion of carboxylic acid 67 to the corresponding primary amide was followed by dehydration with trifluoroacetic anhydride in pyridine to provide nitrile 68.

Table 9. SAR of Compounds with Fused Bicyclic Amines at C7



Cmpds	MIC (μg/mL)		log <i>D</i> <sub>7.4</sub>	p <i>K</i> <sub>a</sub> <sup>b</sup>	hERG QPatch IC <sub>50</sub> (μM) <sup>c</sup>	
	<i>S. aureus</i> FQ-S	<i>S. aureus</i> FQ-R <sup>a</sup>				
48		≤0.03	0.25	-0.68	9.8, 5.2	127 <sup>d</sup>
49		0.06	0.5	-1.03	9.6, 5.2	>300 <sup>e</sup>
50		0.125	1	-1.66	8.6, 5.2	>300
51		≤0.03	1	-1.72	8.4, 4.8	>300
52		≤0.03	0.25	-1.50	8.9, 5.2	>300 <sup>e</sup>
53		0.06	1	-0.40	8.6, 5.2	>300
54		≤0.03	0.06	-1.04	8.9, 5.07	>300
55		≤0.03	0.06	-0.26	8.1, 5.1	>300
56		≤0.03	0.25	-1.28	9.0, 4.9	>300
57		≤0.03	0.125	-0.78	8.5, 5.1	>300

<sup>a</sup>GyrA (S84L); GrIA (S80F); GrIB (E471K). <sup>b</sup>Determined using the UV metric method (see the [Experimental Section](#)). <sup>c</sup>Determined using QPatch automated electrophysiology except for compound 48 (see the [Experimental Section](#) for details). <sup>d</sup>Determined using QPatch automated electrophysiology using a long incubation protocol (see the [Experimental Section](#) for details). <sup>e</sup>Possible solubility issues at higher concentrations.

Buchwald–Hartwig coupling with (±)-**63** yielded **69**, which after Boc deprotection delivered **10**. Nucleophilic addition of hydroxylamine to the nitrile group of **69** gave **70**, which could be cyclized in one of two different ways. Reaction with CDI, followed by Boc deprotection produced **11** in modest yield, while reaction with trimethyl orthoformate and *p*-toluenesul-

fonic acid provided the 1,2,4-oxadiazole **71** in good yield. This intermediate was smoothly deprotected to give **13** in 58% yield.<sup>55</sup>

The preparation of **15** required a different approach in order to install the necessary methylene spacer at C3. Beginning with the carboxylic acid **67**, iododecarboxylation using the

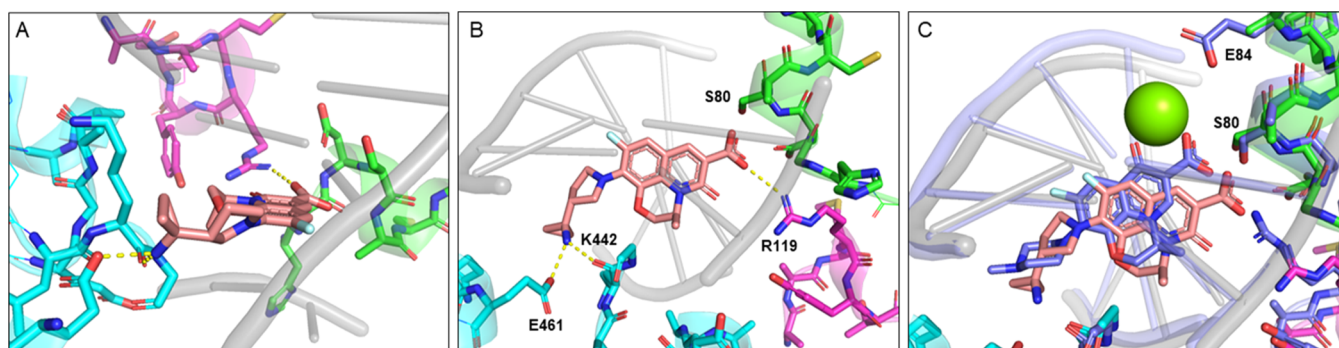


**Figure 2.** Panels (A,B) show the binding site view of the topoisomerase IV ternary complex from *K. pneumoniae* with compound **25** bound (PDB code 7LHZ). DNA nucleotides close to the cleavage site are shown in gray cartoon representation. ParE and ParC residues of one ParE–ParC fusion protein are shown in cyan and green, respectively. ParC residues from the second ParC–ParE fusion protein, which provides R119, are shown in magenta. Residues further out from the binding site were omitted for clarity. Panel (C) shows an overlay with the crystal structure of levofloxacin bound to the topoisomerase IV ternary complex from *K. pneumoniae* (PDB code SEIX). Levofloxacin and the associated DNA and amino acid residues are shown in blue, with the chelated  $Mg^{2+}$  cation shown as a green sphere.

**Table 10. PK Parameters of (–)-8, 24, 25, and 55 in Preclinical Species<sup>a</sup>**

species	(–)-8		24		25		55	
	rat <sup>b</sup>	rat <sup>c</sup>	mouse <sup>d</sup>	rat <sup>e</sup>	dog <sup>f</sup>	rat <sup>g</sup>	rat <sup>g</sup>	rat <sup>g</sup>
CL (mL/min·kg)	5.49	18.5	8.36	3.26	2.48	2.16		
$V_{ss}$ (L/kg)	0.75	1.75	1.88	1.09	1.91	0.52		
$t_{1/2\text{term. iv}}$ (h)	2.56	3.02	3.36	4.64	9.95	3.46		
$AUC_{\text{inf}}$ ( $\mu\text{M}\cdot\text{h}$ )/dose (mg/kg) iv	8.35	2.41	4.68	13.3	17.4	18.6		
$AUC_{\text{inf}}$ ( $\mu\text{M}\cdot\text{h}$ )/dose (mg/kg) po	5.85	1.60	4.30	8.68	19.0	17.5		
$C_{\text{max}}$ ( $\mu\text{M}$ )/dose (mg/kg) po	1.71	0.54	0.49	1.35	1.35	1.70		
$T_{\text{max}}$ p.o. (h)	0.67	0.83	2.0	2.7	4.0	2.0		
oral BA (% F)	70	66	92	65	quant.	97		

<sup>a</sup>All compounds were administered as solutions in the indicated vehicle (see the Experimental Section for details). <sup>b</sup>Hydrochloride salt. Dose = 3.35 mg/kg (iv and po). Vehicle = 20% PEG300 + 5% Solutol in D5W. <sup>c</sup>Hydrochloride salt. Dose = 2.5 mg/kg iv and 5 mg/kg po. Vehicle = 20% PEG300 + 10% Solutol in D5W. <sup>d</sup>Hydrochloride salt. Dose = 2.5 mg/kg iv and 5 mg/kg po. Vehicle = 10% Solutol in D5W. <sup>e</sup>Trifluoroacetate salt. Dose = 2.5 mg/kg iv and 5 mg/kg po. Vehicle = 20% PEG300 + 5% Solutol in D5W. <sup>f</sup>Hydrochloride salt. Dose = 0.125 mg/kg iv and 1 mg/kg po. Vehicle = 10% Solutol in D5W. <sup>g</sup>Hydrochloride salt. Dose = 1 mg/kg iv and 3 mg/kg po. Vehicle = 20% PEG300 + 20% Solutol in D5W.

conditions developed by Montoir *et al.*<sup>56</sup> provided the C3 iodide in good yield, which could be readily displaced with dimethyl malonate to give **72** (Scheme 4). Ester hydrolysis, decarboxylation, and subsequent re-esterification proceeded smoothly and provided access to **73**. Buchwald–Hartwig

coupling with **63** and subsequent formation of the acylhydrazide using hydrazine in EtOH/water provided **74** in 75% yield over the two steps. Final cyclization with triphosgene and Boc deprotection gave compound **15**.

Synthesis of the C4-substituted analogues described in Table 3 utilized triflate **75** as a common intermediate (Scheme 5).<sup>33</sup> This C4 triflate proved to be highly reactive and chemoselectivity in cross-coupling reactions over the C7 bromide was readily achieved. In this way, Sonogashira coupling<sup>57,58</sup> with ethyl propynoate provided **76**, which upon treatment with hydroxylamine and NaOH at 0 °C formed the desired 3-hydroxyisoxazole **77** in high yield.<sup>59</sup> Temporary protection of the acidic hydroxyl was necessary to enable Buchwald–Hartwig coupling with **63**. Final deprotection with HCl gave **16**.

The synthesis of related analogues **17** and **18** is shown in Scheme 6, depicted as parallel sequences. Beginning with the C4 triflate **75**, Negishi cross-coupling with  $Zn(CN)_2$  cleanly provided nitrile **78**.<sup>60</sup> Buchwald–Hartwig coupling with **63** gave **79**, which then underwent nucleophilic addition of hydroxylamine to the C3 nitrile group. Cyclization with thio-CDI led to **80**, and final Boc deprotection afforded **17**. Alternatively, Pd-catalyzed carbonylation<sup>61</sup> of **75** gave ethyl ester **81**, which underwent the usual Buchwald–Hartwig coupling with **63**. Formation of the C4 acyl hydrazide intermediate and cyclization with triphosgene in a manner analogous to compound **15** provided the desired oxadiazolone heterocycle (**73**). Final deprotection with HCl delivered **18**.

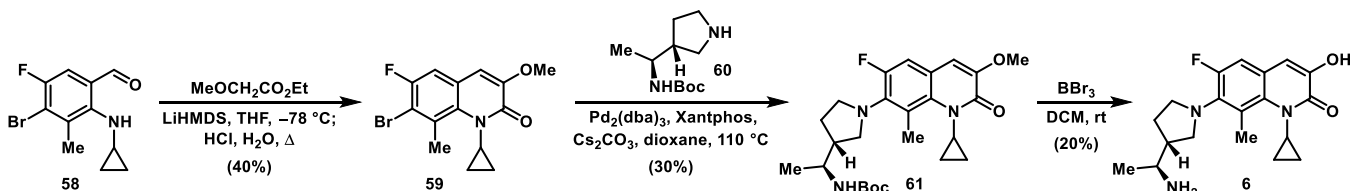
Synthesis of C4-substituted analogues featuring a methylene spacer is described in Schemes 7–9. Stille coupling<sup>62,63</sup> between **75** and vinyl stannane **84** provided **85** in 84% yield

**Table 11. In Vivo Efficacy of (–)-8, 24, 25, 55, and Moxifloxacin against FQ-S *S. aureus* and a FQ-R *S. aureus* Clinical Isolate in a Neutropenic Murine Thigh Infection Model<sup>a</sup>**

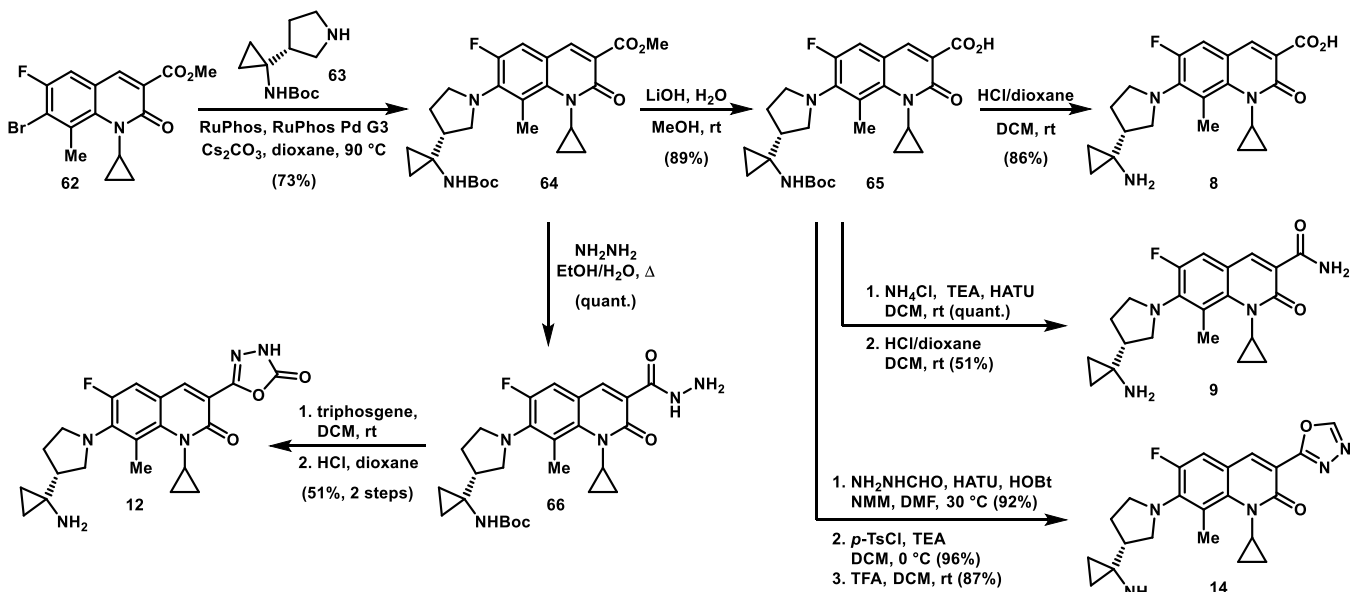
	(–)-8	24	25	55	moxifloxacin
PPB (% bound, m/r/h)	51/70/79	6/28/20	13/37/24	59/58/82	24/31/19
<i>S. aureus</i> FQ-S MIC ( $\mu\text{g/mL}$ )	0.06	0.25	0.25	0.03	0.06
static dose (mg/kg/day)	4	NT	3	7	14
<i>S. aureus</i> FQ-R clinical isolate MIC ( $\mu\text{g/mL}$ )	1	2	4	0.5	8
static dose (mg/kg/day)	NT	68	27	NT	NT

<sup>a</sup>Compounds were administered subcutaneously. See the Experimental Section for details on *in vivo* studies. See Table 13 for a description of bacterial strains used.

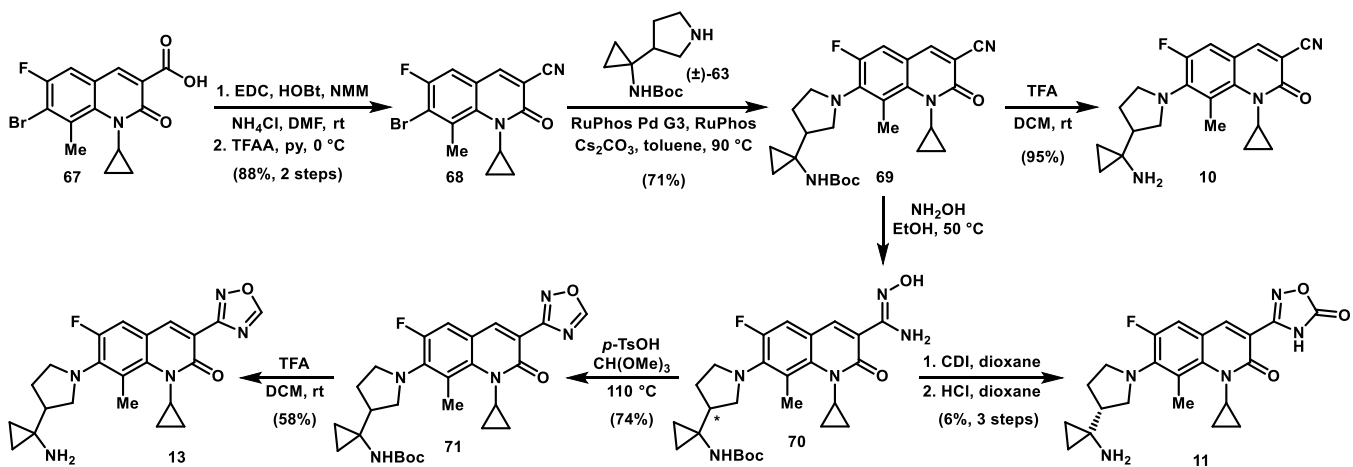
Scheme 1. Synthesis of Compound 6



Scheme 2. Synthesis of Compounds 8, 9, 12, and 14



Scheme 3. Synthesis of Compounds 10, 11, and 13

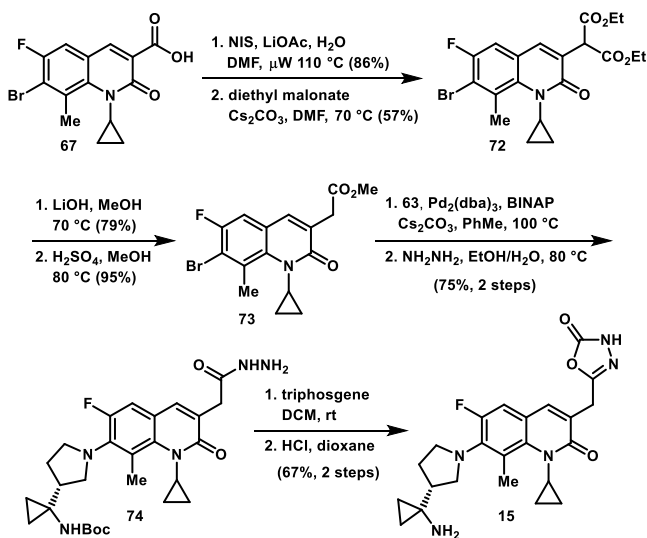


(Scheme 7).<sup>64</sup> The enol ether was cleaved with TFA to reveal the corresponding aldehyde, which was subsequently converted to the methyl ester (86) *via* Pinnick oxidation and esterification.<sup>65–68</sup> Introduction of the C7 amine proceeded in modest yield, before hydrolysis generated the requisite carboxylic acid (88). Compound 88 was then subjected to a Masamune–Claisen condensation, providing keto-ester 89 in reasonable yield.<sup>69</sup> Condensation with hydroxylamine generated the hydroxyisoxazole ring (90),<sup>70</sup> and deprotection with HCl completed the synthesis of 19.

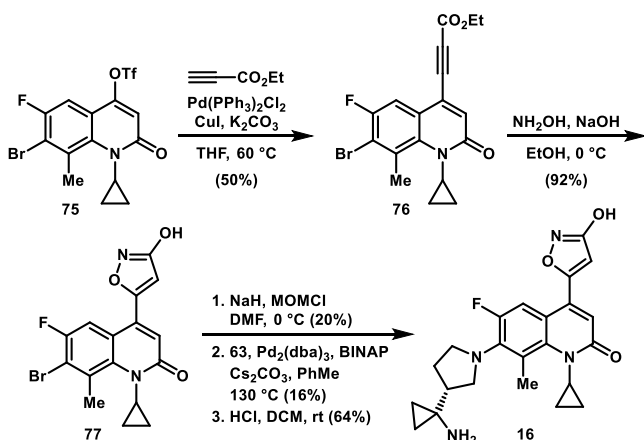
Once again utilizing key intermediate 75, Suzuki–Miyaura<sup>71,72</sup> coupling with vinylboronic acid pinacol ester

generated 91, which was subjected to oxidative cleavage, reduction, and *tert*-butyldimethylsilyl (TBS) protection to give 92 (Scheme 8a). Buchwald–Hartwig coupling with 63 produced 93, followed by TBS removal with tetra-*n*-butylammonium fluoride (TBAF) and formation of the benzylic mesylate 94. Displacement of the mesylate with cyanide was effected by the hypervalent cyanosilicate derived from trimethylsilyl cyanide and TBAF,<sup>73</sup> and subsequent reaction with hydroxylamine gave amidoxime 95. A two-step procedure was employed to generate the 5-thio-1,2,4-oxadiazole ring.<sup>74</sup> The amidoxime was first treated with acetic anhydride and triethylamine to effect O-acylation. The

Scheme 4. Synthesis of Compound 15

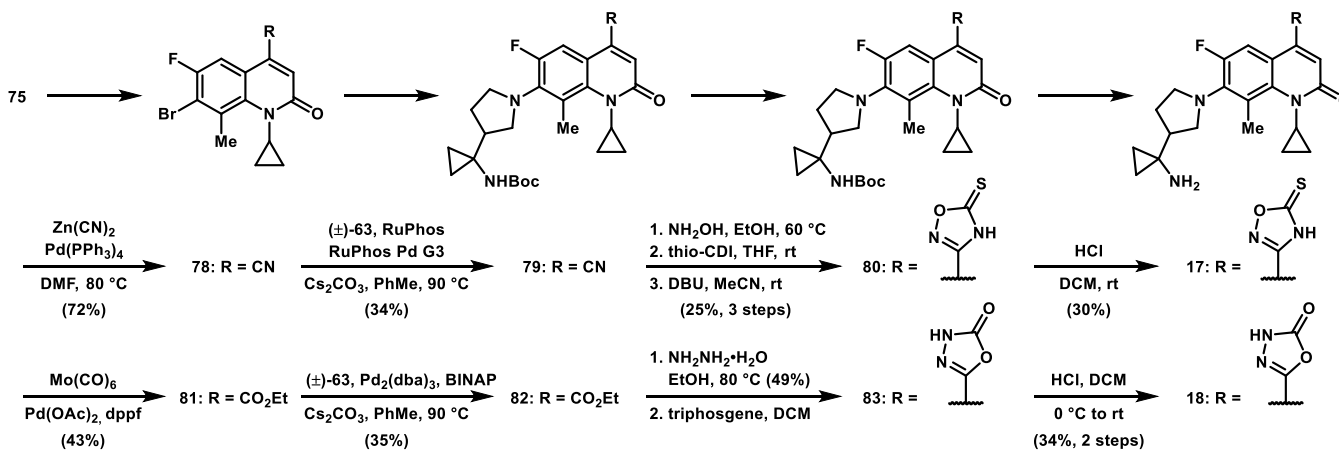


Scheme 5. Synthesis of Intermediate 16



intermediate was then reacted with carbon disulfide and NaH to give **96** before Boc deprotection with HCl to afford **20**. Compound **21** was also prepared from **95** using an analogous route, using CDI instead to form the 1,2,4-oxadiazolone ring in **97** prior to Boc deprotection with TFA (Scheme 8b).

Scheme 6. Synthesis of Intermediate 17 and 18

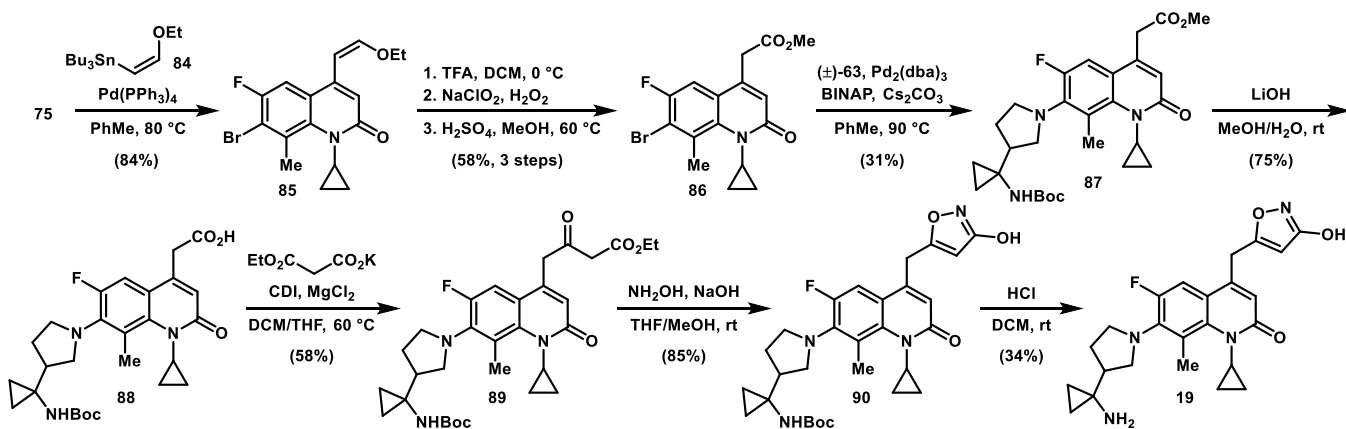


The synthesis of **22**, containing a 1,3,4-oxadiazol-2-one heterocycle, was initiated from intermediate **87** and employed the same sequence of steps that was used to access **18** (i.e., **82** → **83** → **18**, Scheme 9a). Finally, amide **23** was derived from the corresponding carboxylic acid (**88**) using conventional methods (Scheme 9b).

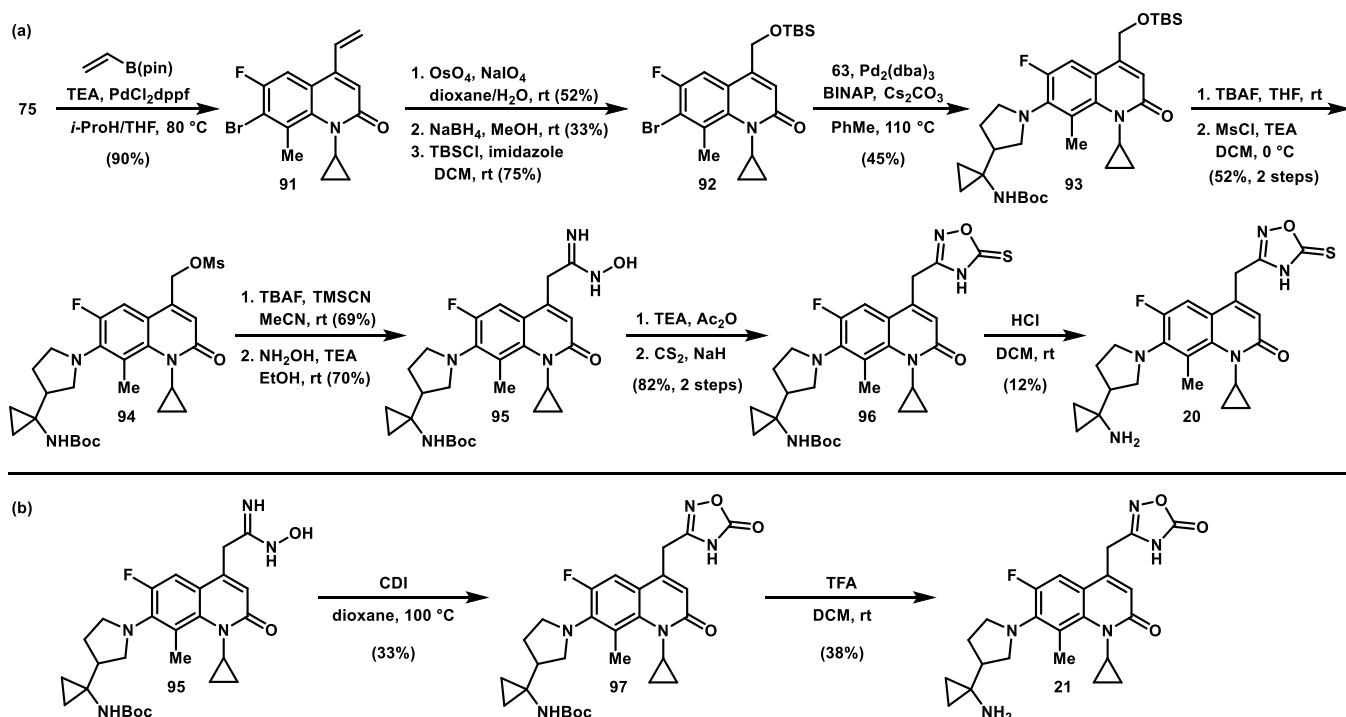
Initial studies of compound **24** and related analogues made use of a 17-step synthetic route outlined in Scheme 10a. Key intermediate **99** (described previously)<sup>33</sup> was subjected to a copper-catalyzed Ullman coupling with NaOMe in MeOH to introduce the necessary oxygenation at what would become the C8 position.<sup>75</sup> This reaction was accompanied by significant ester hydrolysis, necessitating an esterification step to provide **101**. The Sandmeyer reaction<sup>76,77</sup> under aqueous conditions afforded iodide **102**, which underwent methyl ether cleavage in the presence of BBr<sub>3</sub> to provide phenol **103**. Synthesis of the benzoxazine derivative **106** leveraged methodology developed previously by Bower *et al.* for the synthesis of levofloxacin.<sup>78</sup> Thus, deprotonation of **103** with NaH and alkylation with chiral sulfamidate **104** cleanly provided **105**, which in turn underwent an intramolecular Buchwald–Hartwig amination to yield **106**. Acylation of the aniline with methylmalonyl chloride was carried out in the absence of a base to generate morpholine **107**; subsequent cyclization was then realized with Cs<sub>2</sub>CO<sub>3</sub> in acetonitrile to afford tricycle **108** in good yield. Triflate **109** was then obtained following brief treatment with triflic anhydride and triethylamine. The labile nature of this intermediate necessitated immediate Pd-catalyzed reduction to provide **110**.<sup>79–82</sup> Buchwald–Hartwig coupling with **60** was followed by ester hydrolysis and Boc deprotection to furnish **24**. Compound **25** was obtained in an analogous manner (Scheme 10b).

While the route described in Scheme 10 offered substantial flexibility and was amenable to gram-scale synthesis of **25**, we required a shorter and more scalable route for ongoing studies of this compound. To this end, we devised and implemented an improved synthetic approach shown in Scheme 11. Bromination of **115** provided **116**, which was alkylated as before with cyclic sulfamidate **104** using modified conditions [*t*-BuOK, dimethylformamide (DMF), 40 °C] and subjected to intramolecular Buchwald–Hartwig amination that proceeded in 69% yield. A second bromination with *N*-bromosuccinimide provided **119**. Lithium–halogen exchange followed by formylation using *N*-formylmorpholine as a formyl

Scheme 7. Synthesis of Intermediate 19



Scheme 8. Synthesis of Intermediate 20 and 21



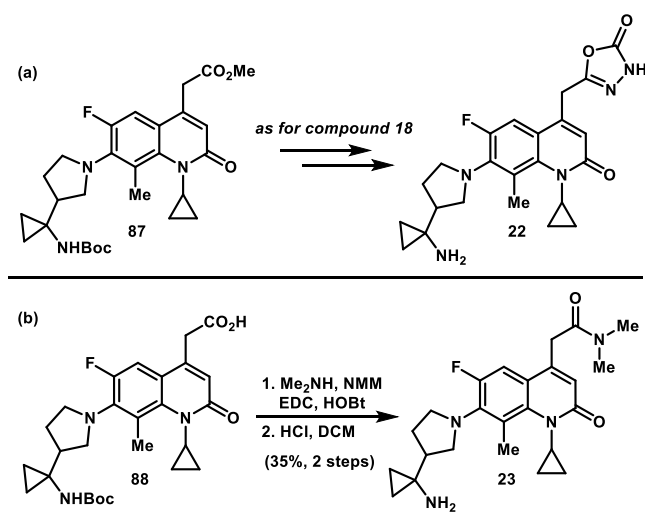
donor gave the desired aldehyde **120** in 51% yield, along with recovered starting material.<sup>83</sup> Condensation with dimethyl malonate directly provided the key tricyclic intermediate **121** in good yield. Introduction of the C7 amine was now performed by simple  $S_NAr$  reaction with pyrrolidine **63**. Standard hydrolysis and Boc deprotection delivered **25** in 88% yield over the final three steps and only nine total steps from **115**. As a testament to the much improved efficiency of the newly developed strategy, this route proved amenable to the preparation of >700 g of **25**.

Subsequently, and in anticipation of future material needs, we developed a shorter and more efficient synthesis of key intermediate **121** (Scheme 12). To this end, it was found that by maintaining the temperature of the initial bromination reaction at  $-35$  °C, the isolated yield of **116** could be improved to 67%. Conversion of **116** to **117** proceeded uneventfully as before. Reducing the duration of heating for the subsequent intramolecular Buchwald–Hartwig reaction resulted in an improved yield of 81% for compound **118**

following silica gel chromatography. At this stage, the new route diverged from that described in Scheme 11. Acylation of **118** with methyl malonyl chloride provided **122**, which was not isolated but submitted directly to a condensation reaction with paraformaldehyde to give **123**. Electrophilic aromatic cyclization could be induced in the presence of  $AlCl_3$  at ambient temperature to produce the corresponding dihydropyridone, which was immediately oxidized with 2,3-dichloro-5,6-dicyano-1,4-benzoquinone (DDQ) to the desired product **121**. The sequence of reactions from **118**  $\rightarrow$  **121** could be effectively telescoped and thus provided **121** in 16% overall yield from **115** with only two chromatography steps (**116** and **118**). This route ultimately enabled the synthesis of >1 kg of key intermediate **121**.

The synthesis of analogues with modifications to the lower ring of the tricyclic core relied on slight modifications of the route described in Scheme 10. For example, compounds **26** and **27** were accessed using this protocol and simply substituting **104** with the appropriate cyclic sulfamidate.

Scheme 9. Synthesis of Compounds 22 and 23

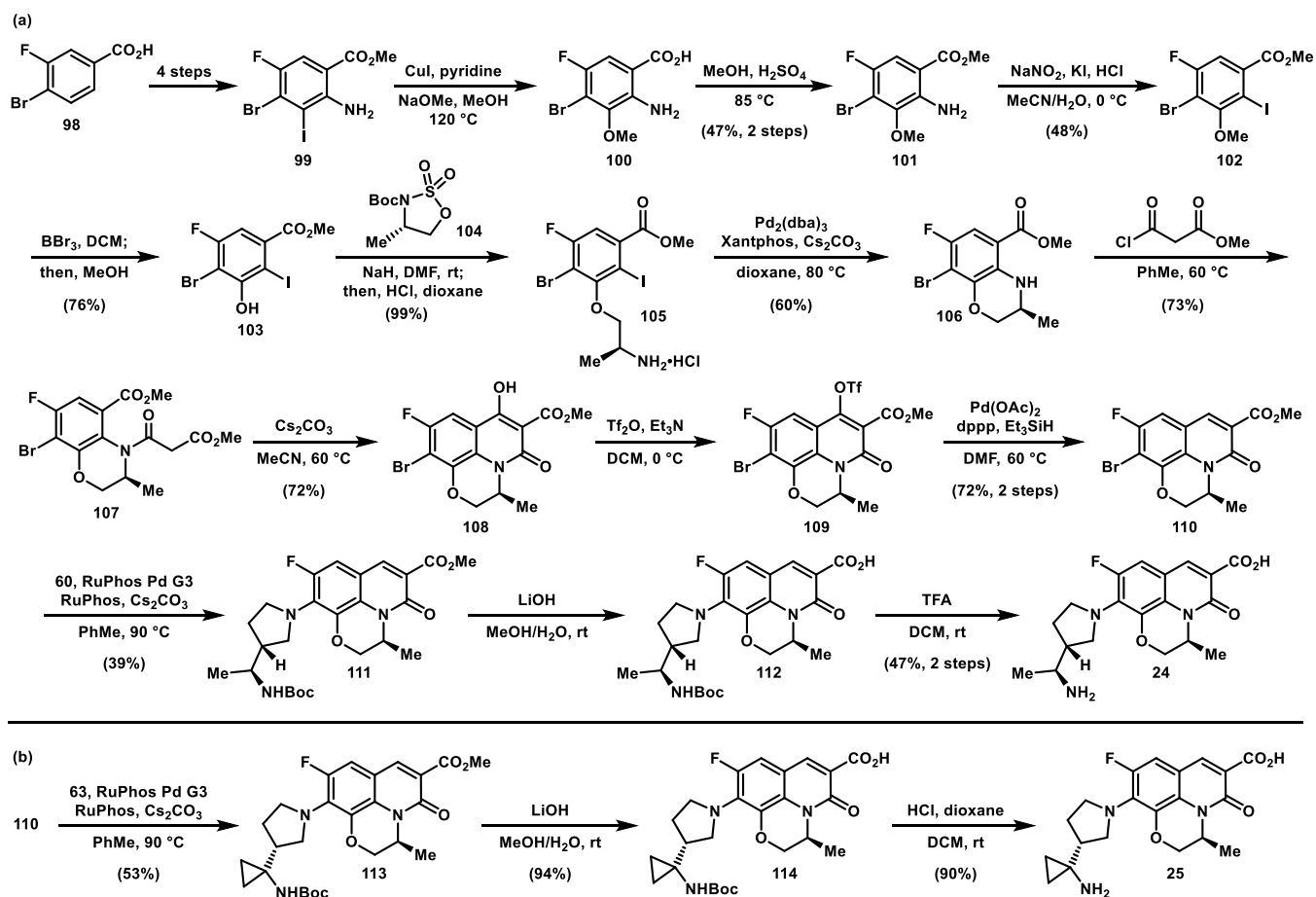


Compound 28 required more extensive modifications to the route (Scheme 13a). Thus, Sonogashira coupling between iodide 99 and alkyne 124 provided 125 in high yield. Reduction of the alkyne proved remarkably challenging in the presence of the Boc group; as such, the protecting group was removed prior to hydrogenation with Adams' catalyst then reinstalled to give 127. Diazotization of the aniline was carried out under neutral conditions with nitrosonium tetrafluorobo-

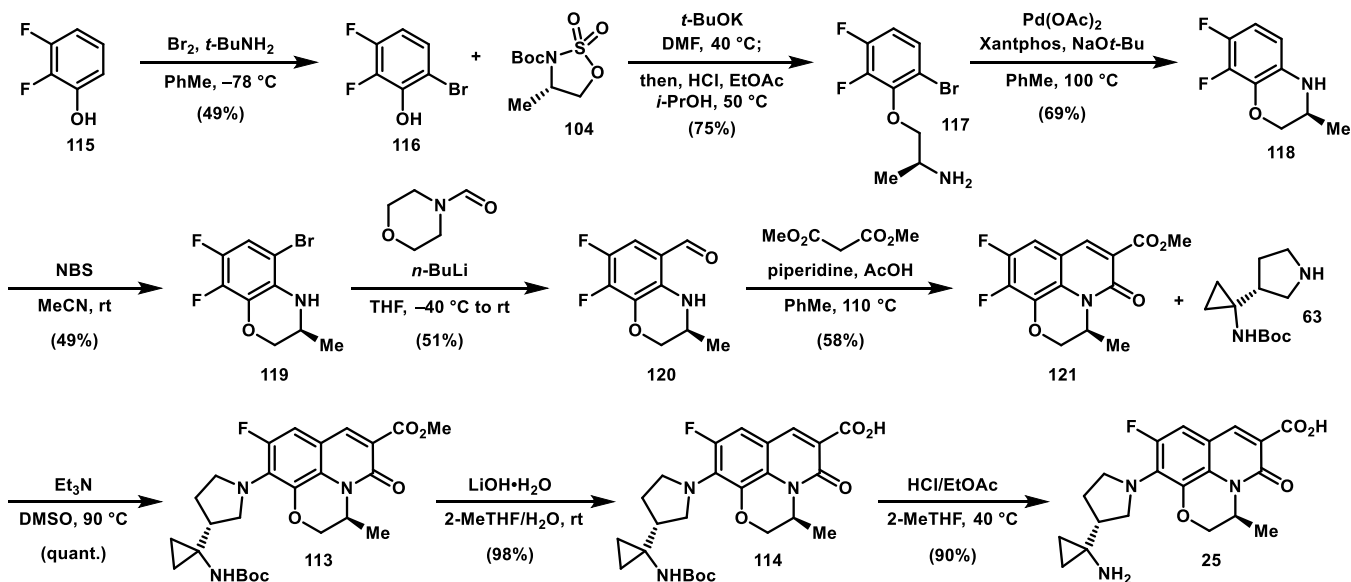
rate; treatment of the resulting diazonium salt with KI in the presence of dibenzo-18-crown-6 furnished the desired iodide in reasonable yield. Removal of the Boc group once more allowed for a high-yielding intramolecular Buchwald–Hartwig amination to provide 129. The remaining steps in the sequence mirrored those in Scheme 10 for the preparation of 25. The five-membered ring analogue 29 was subsequently prepared as shown in Scheme 13b. Sonogashira coupling with propyne gave 134, which underwent smooth hydroamination/cyclization to provide the desired indole 135.<sup>84</sup> Ionic reduction of the indole<sup>85,86</sup> led to 136, which was carried through a seven-step sequence analogous to 28 to afford compound 29.

Introduction of functionality at the C5 position of 25 was realized by taking advantage of the innate nucleophilicity at this position in the tricyclic scaffold. In this way, nitration of 110 gave 137, which could be converted to the fluorinated derivative 138 upon treatment with tetramethyl ammonium fluoride (TMAF) in DMF at room temperature. Notably, TMAF was found to be far superior to other sources of fluoride for this transformation.<sup>87,88</sup> Reduction of the nitro group to aniline 139 and re-esterification of the intermediate provided 140 (Scheme 14). Both 138 and 140 underwent the three-step sequence including Buchwald–Hartwig amination, ester hydrolysis, and Boc deprotection, as described for 25 (see Scheme 10b) to produce 30 and 32, respectively. Similarly, halogenation of 110 at C5 was successful with either *N*-chloro or *N*-iodosuccinimide to afford 141 and 142, respectively (Scheme 15). Negishi cross-coupling with 142 and Zn(CN)<sub>2</sub>

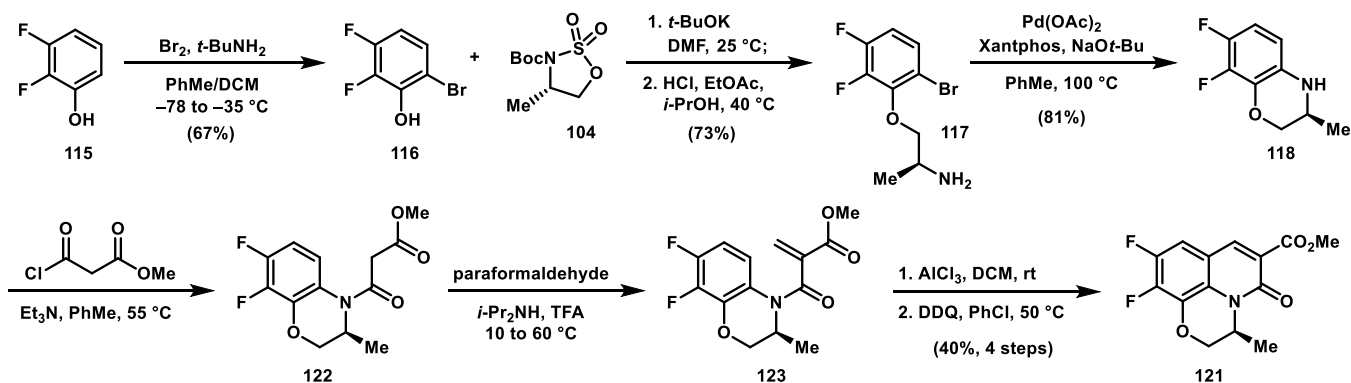
Scheme 10. Initial Synthesis of Compounds 24 and 25



Scheme 11. Process Chemistry Route to 25



Scheme 12. Alternative Process Chemistry Route to Intermediate 121 for the Synthesis of 25



gave **143**. Once again, chloride **141** and nitrile **143** were progressed to the final analogues **31** and **33** using the previously described sequence (see [Scheme 10b](#)).

Preparation of the C6 des-fluoro analogue **34** required starting from phenol **144**, which underwent alkylation with **104** as expected in good yield. In this case, following removal of the Boc group, the resulting amine underwent intramolecular  $S_NAr$  reaction upon warming in DMF, providing **146**. Redox manipulation of the ester proceeded uneventfully to give aldehyde **148**, which was condensed with dimethyl malonate to provide **149**. Final compound **34** was accessed in three steps, as previously described (see [Scheme 10b](#)). This general route was applied to the synthesis of C6–H analogues featuring substituents at C5 ([Scheme 17](#)). Bromination of phenol **150** provided **151**, which was in turn subjected to the sequence outlined in [Scheme 16](#), delivering compound **35**. Likewise, compounds **36** and **37** were accessed in the same manner, simply substituting the appropriate starting material for **150**.

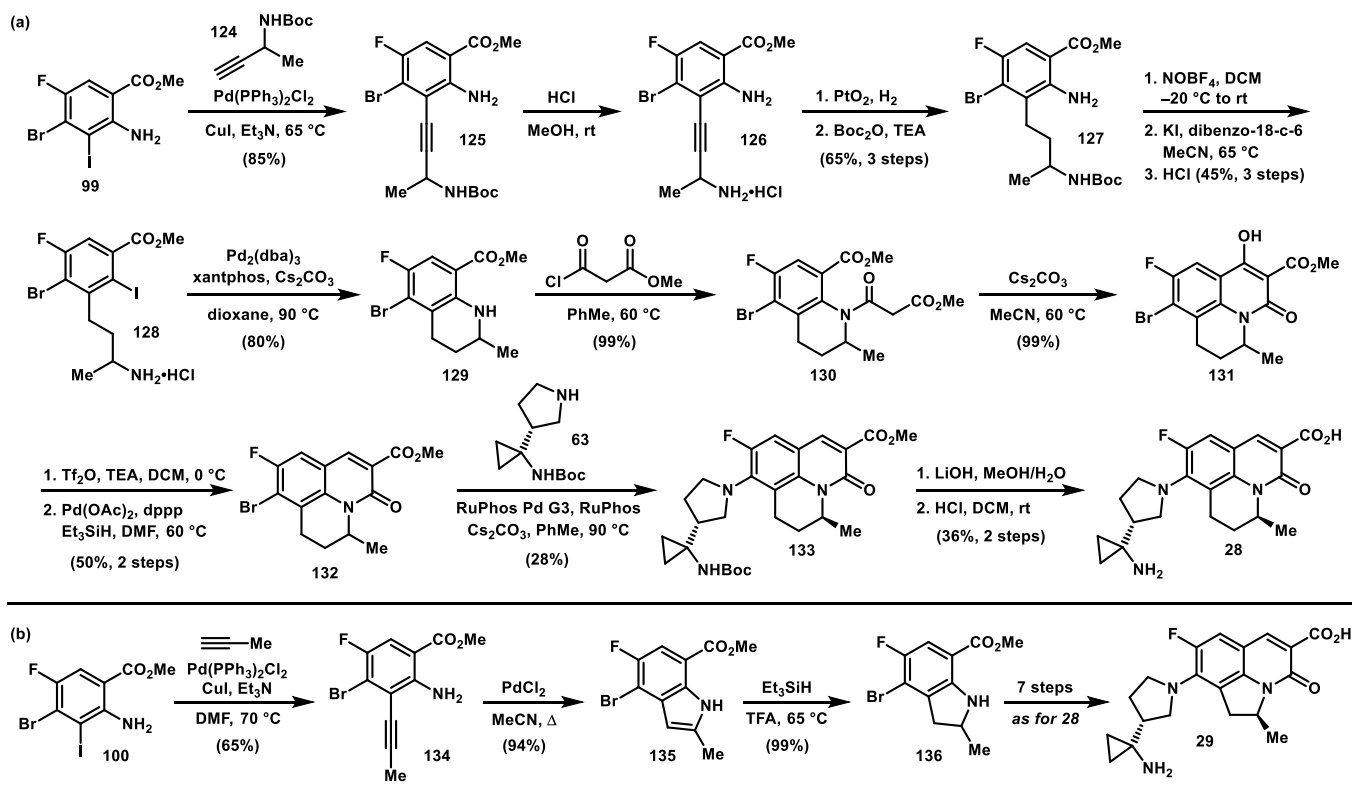
During the synthesis of compounds **30** and **32**, it was observed that the C6 fluorine in intermediate **137** could be readily displaced by a variety of nucleophiles. This reactivity was harnessed to access C6 analogues **38–40**. For example, treating **137** with ammonium carbonate at elevated temperatures provided access to aniline **152** ([Scheme 18](#)).

Diazotization of the aniline<sup>89</sup> followed by reaction with CuCN provided nitrile **154** in reasonable yield. The C5 nitro group was then eliminated in three steps: reduction to the aniline (**155**), diazotization, and finally, hydrodediazonation of **156** with FeSO<sub>4</sub> in DMF.<sup>90</sup> The resulting intermediate **157** was advanced to **38** using the standard protocols previously described (see [Scheme 10b](#)). Diazonium salt **153** could also be successfully converted to the corresponding chloride (**158**), which provided the basis for synthesis of compound **39** ([Scheme 19](#)). Compound **40**, on the other hand, was accessed by displacement of the C6 fluorine in **137** with sodium methoxide. The resulting intermediates (**158** and **159**) were advanced to **39** and **40**, respectively, using the sequence described for **38** (*i.e.*, **154** → **38**, [Scheme 18](#)).

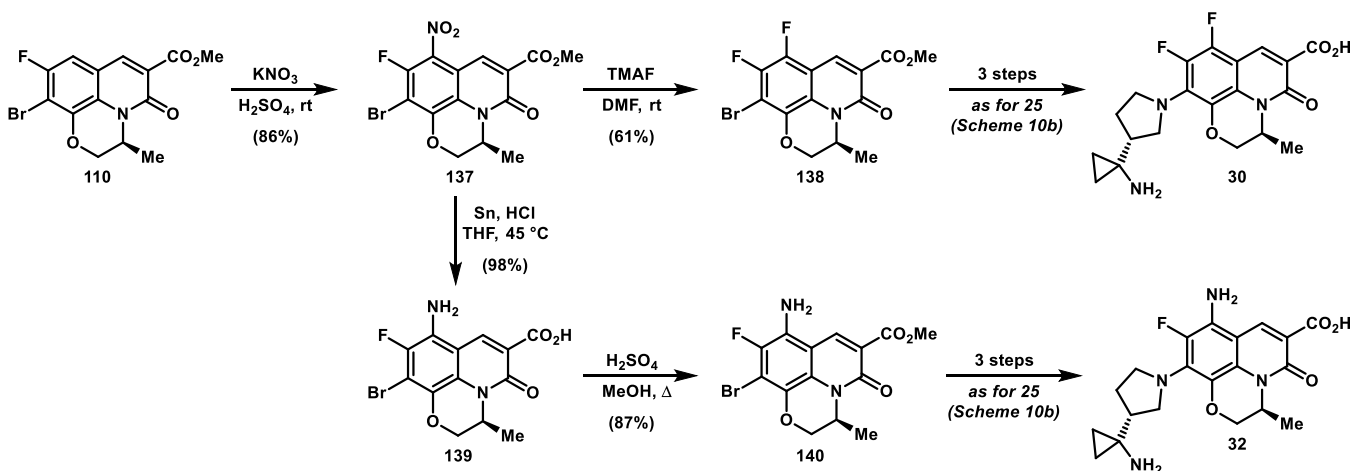
The C7 analogues described in [Table 8](#) (*i.e.*, **41–47**) were uniformly prepared by Buchwald–Hartwig coupling reactions between **110** and the appropriate cyclic amine, as described for **25**. In all cases, the amines used were commercially available, with the exception of compound **45**. In this case, the cross-coupling partner **161** was prepared from known compound **160**,<sup>44</sup> as shown in [Scheme 20](#). Coupling with **110** proceeded in 84% yield to give **162** and was followed by silyl group removal with TBAF. Mesylation of the resulting allylic alcohol and displacement with azide then gave **164**. Staudinger



Scheme 13. Synthesis of Compounds 28 and 29



Scheme 14. Synthesis of Compounds 30 and 32



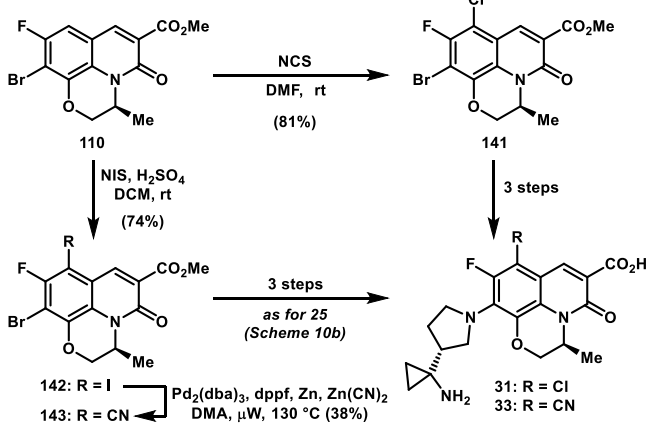
reduction of the azide and ester hydrolysis then provided allylic amine **45**.

Compounds containing bicyclic amines at *C7* were generally assembled by first constructing the 5-6-fused bicyclic systems using different synthetic strategies and appending the resulting pyrrolidines to the fluoroquinolone core at a late stage. For instance, the *cis*-fused bicyclic framework of pyrrolidine **170** was built from cyclohexenone (**166**) *via* a 1,3-dipolar cycloaddition reaction with *N*-benzylazomethine ylide, generated *in situ* by treatment of *N*-benzyl-1-methoxy-*N*-((trimethylsilyl)methyl)methanamine with catalytic TFA (Scheme 21).<sup>91,92</sup> The resulting ketone **167** was subjected to a reductive amination with ammonium acetate, which after Boc-protection, afforded a 3:1 mixture of diastereomers at *C3'*, separable by column chromatography. At this stage, the major

diastereomer was again purified by chiral supercritical fluid chromatography (SFC) to obtain **168** as a single enantiomer, from which the benzyl group was removed under transfer hydrogenation conditions to reveal the free pyrrolidine. Buchwald–Hartwig amination with **170** then proceeded smoothly under the previously established conditions with bromide **110** to afford methyl ester **171** in 66% yield. A final hydrolysis and Boc-deprotection then provided the *C7*-bicyclic amine derivative **48**.

Synthesis of the *trans*-fused bicyclic amine required an entirely different synthetic approach. Here, the 1,3-dipolar cycloaddition reaction was carried out with *E*-butadiene **172**, thus providing *N*-benzyl pyrrolidine **173** with the desired *trans* configuration between the vinyl and ester groups (Scheme 22). We observed that the basic amine in **173** frequently

Scheme 15. Synthesis of Compounds 31 and 33



contributed to difficult purifications and accompanying low product recovery in subsequent reactions. To circumvent this problem, it was found that conversion of **173** to benzyl carbamate **174** much improved downstream compound handling. Next, redox manipulation of the ester afforded aldehyde **175**, which enabled condensation with *rac*-*tert*-butanesulfinamide and 1,2-addition of allyl magnesium bromide into imine **176**. After Boc-protection of the resulting primary amine, C3' diastereomers **178** and **179** were separated by column chromatography in a combined 79% yield over the three steps. The minor diastereomer was then engaged in a ring-closing metathesis reaction to forge the *trans*-fused 5,6-bicyclic system, which after hydrogenation delivered deprotected pyrrolidine **181**. This racemic intermediate was then installed on the enantiopure fluoroquinoline core *via*  $S_NAr$  with difluoroarene **121** to produce a mixture of diastereomers that were separated by chiral SFC following ester hydrolysis. A final Boc-deprotection afforded **49** as the stereochemical complement to **48**.

Introducing oxygen into the six-membered ring necessitated yet another synthetic route redesign to construct the bicyclic system. Aldehyde **183** underwent condensation and chlorination to give nitrile oxide-precursor **184**, which engaged in a dipolar cycloaddition reaction with dipolarophile **185** to afford dihydroisoxazole **186** (Scheme 23). Reductive cleavage of the N–O bond in the newly-formed ring and imine reduction revealed the primary amine, which was Boc-protected before separating the diastereomers formed at C3'. The minor diastereomer **188** was treated with TBAF to afford diol **190**, in which the primary alcohol was selectively mesylated and attacked by the pendant secondary alcohol to form the *cis*-fused pyran ring system. Hydrogenolysis using Pearlman's catalyst gave pyrrolidine **192** that engaged in an  $S_NAr$  reaction with **121**, as before. The resulting diastereomers of **193** were

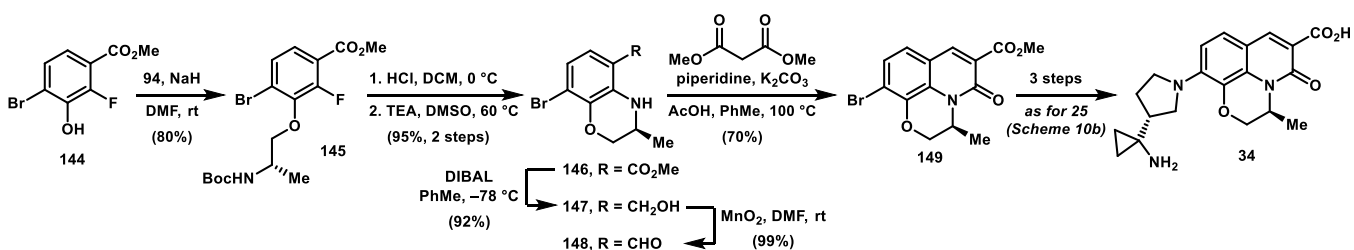
separated by chiral SFC, hydrolyzed, and deprotected to furnish *cis*-fused pyran **50**.

The *trans*-fused bicyclic system was accessed from commercially available pyrrolidine **194** (Scheme 24). Treatment with vinyl magnesium chloride in the presence of CuBr·dimethylsulfide effected epoxide opening to afford **195** in 94% yield. The resulting secondary alcohol was alkylated with allyl bromide, thus enabling dihydropyran formation *via* ring-closing metathesis. The double bond in **197** was leveraged to install the remaining necessary oxidation state at C3'. To this end, epoxidation with meta-chloroperoxybenzoic acid (*m*-CPBA) delivered **198** as a 2:1 mixture of diastereomers, favoring the desired configuration. The epoxide was opened with diisobutylaluminum hydride (DIBAL) at the less hindered site, and the resulting alcohol **199** was mesylated and displaced with sodium azide; inversion *via* this sequence ensured the desired stereochemistry would be obtained at C3'. Azide **200** was then reduced under hydrogenation conditions to reveal the primary amine, which was subsequently protected as the allyl carbamate in order to allow orthogonal deprotection of **202** to afford free pyrrolidine **203**.  $S_NAr$ , chiral SFC separation, and hydrolysis proceeded as before, followed by a final alloc-deprotection mediated by Pd(PPh<sub>3</sub>)<sub>4</sub> to deliver *trans*-pyran **51**.

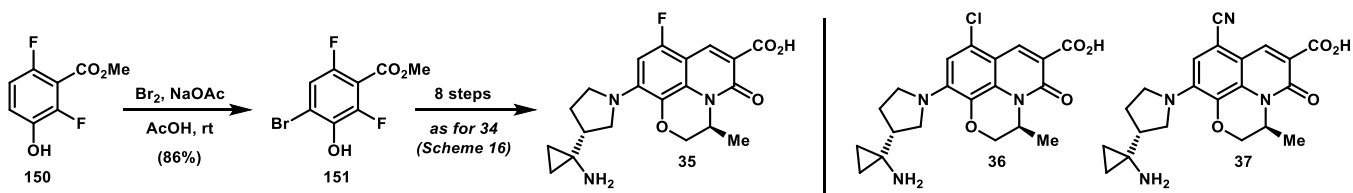
Functional groups at C5' of the six-membered ring were introduced by utilization of a Diels–Alder reaction between *N*-benzylmaleimide and siloxy diene **206**, prepared from (*E*)-4-methoxybut-3-en-2-one (**205**, Scheme 25).<sup>93,94</sup> This strategy permitted rapid access to *cis*-fused bicyclic **208**, containing both an oxidative handle at C5' and amine functionality with the desired stereochemistry at C3'. Selective double debenzoylation and reprotection as the Boc carbamate provided imide **209**, which was sequentially reduced over two steps to pyrrolidine **210** in 94% yield. Following the established  $S_NAr$  and silyl deprotection, alcohol **211** proved a versatile intermediate that could be advanced in a divergent fashion. First, methylation of **211** with methyl iodide in the presence of silver oxide led to methoxy derivative **52**. Second, fluorine was incorporated in a variety of ways: difluoromethoxy derivative **53** was prepared from **211** by reaction with difluorocarbene, generated from 2,2-difluoro-2-(fluorosulfonyl)acetic acid,<sup>95,96</sup> to give intermediate **213** in 52% yield. Alternatively, treatment of **211** with diethylaminosulfur trifluoride (DAST) effected deoxyfluorination, albeit in low yield, leading to monofluoride **54**, while oxidation to ketone **214** allowed synthesis of the corresponding gem-difluoro analogue **55**.

Protected enone **216** provided a convenient starting point to incorporate 1,4-functionality across the six-membered ring. Luche reduction and methylation provided methoxy enone **217**, which was engaged as before in a 1,3-dipolar cycloaddition to afford a 3:1 mixture of diastereomers **219** and **218**,

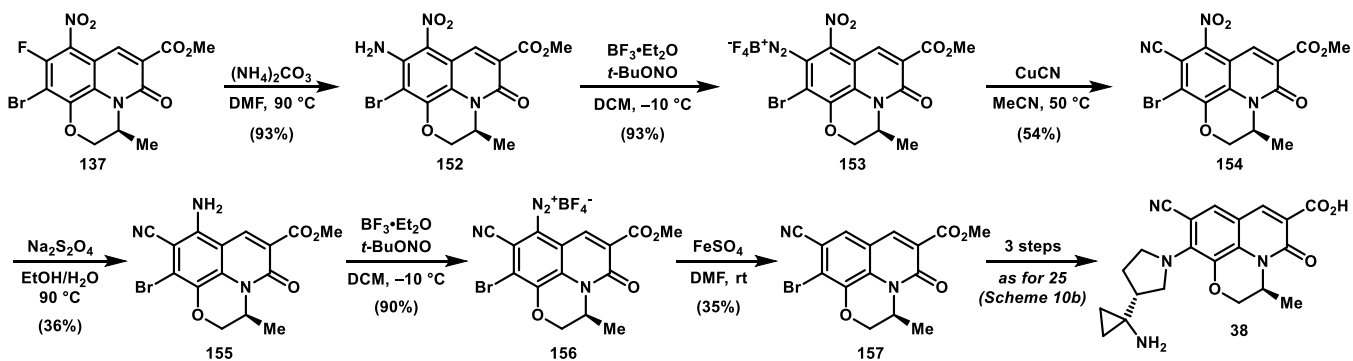
Scheme 16. Synthesis of Compound 34



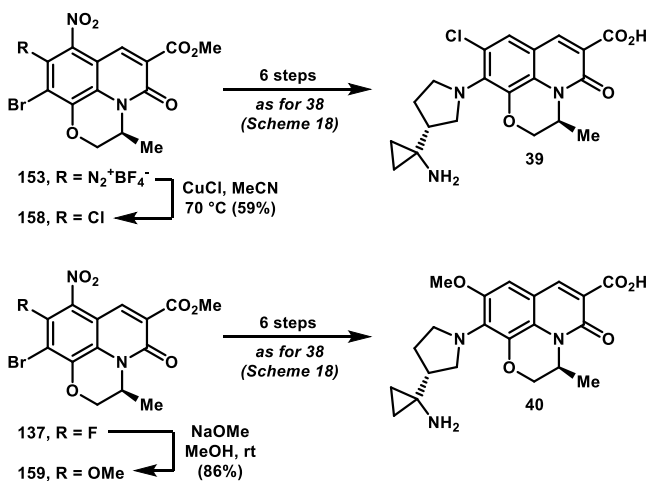
Scheme 17. Synthesis of Compounds 35–37



Scheme 18. Synthesis of Compound 38

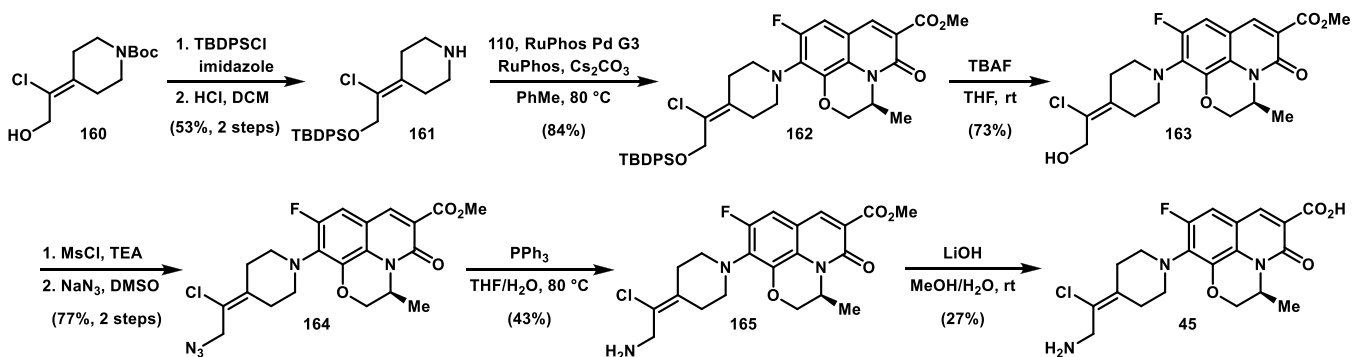


Scheme 19. Synthesis of Compounds 39 and 40



respectively (Scheme 26). The primary amine was again installed *via* reductive amination with ammonium acetate; however, the resulting diastereomers at C3' required high-performance liquid chromatography (HPLC) purification to achieve separation, even after Boc-protection. Nonetheless, 6'-

Scheme 20. Synthesis of Compound 45



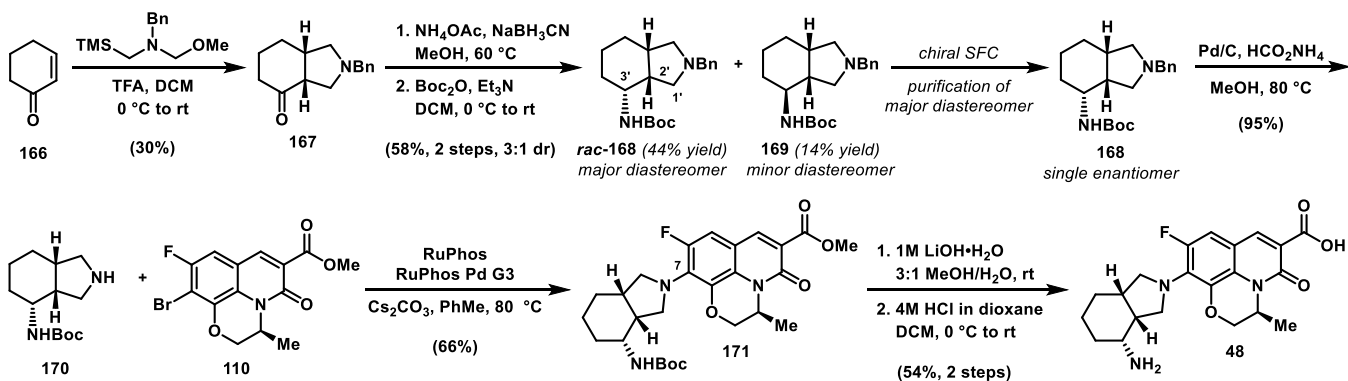
methoxy-substituted bicycle 221 was debenzylated in high yield to give pyrrolidine 222, which was elaborated through the usual late-stage sequence to furnish 56.

Finally, 57 was also constructed from 216, this time with the dipolar cycloaddition reaction proceeding at the outset of the synthetic sequence (Scheme 27). Reductive amination from the convex face of 224, followed by acidic deprotection of the dioxolane, provided amino ketone 225 as a single diastereomer. Boc-protection, 1,2-reduction, and hydrogenolysis proceeded uneventfully under standard conditions to afford pyrrolidine 228, which after  $S_NAr$  with 121, provided a similarly useful alcohol intermediate analogous to 211 that was leveraged for further functional group manipulations at C6' (not shown). Lastly, the end game strategy used for 55 was applied, wherein Dess–Martin periodinane oxidation provided ketone 229, which underwent deoxyfluorination, hydrolysis, and deprotection to furnish gem-difluoro analogue 57.

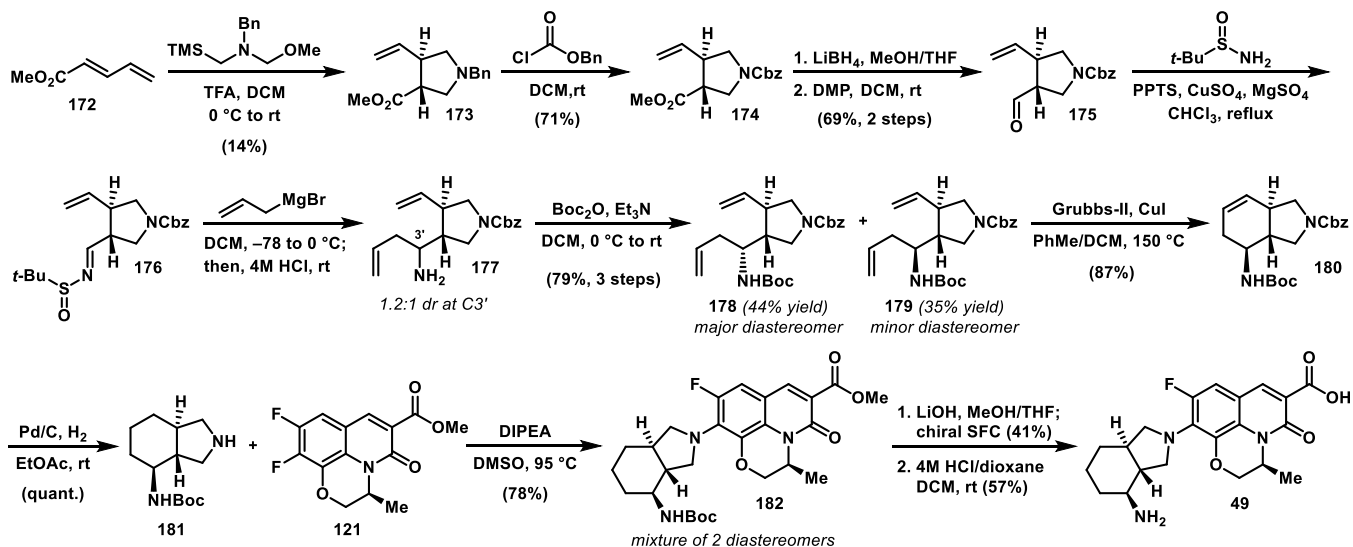
## CONCLUSIONS

The need for novel antibiotics to treat serious, resistant bacterial infections continues to grow as mainstay therapies see their efficacy eroded with each passing year. Quinolones have proven to be one of the most successful classes of antibiotics to

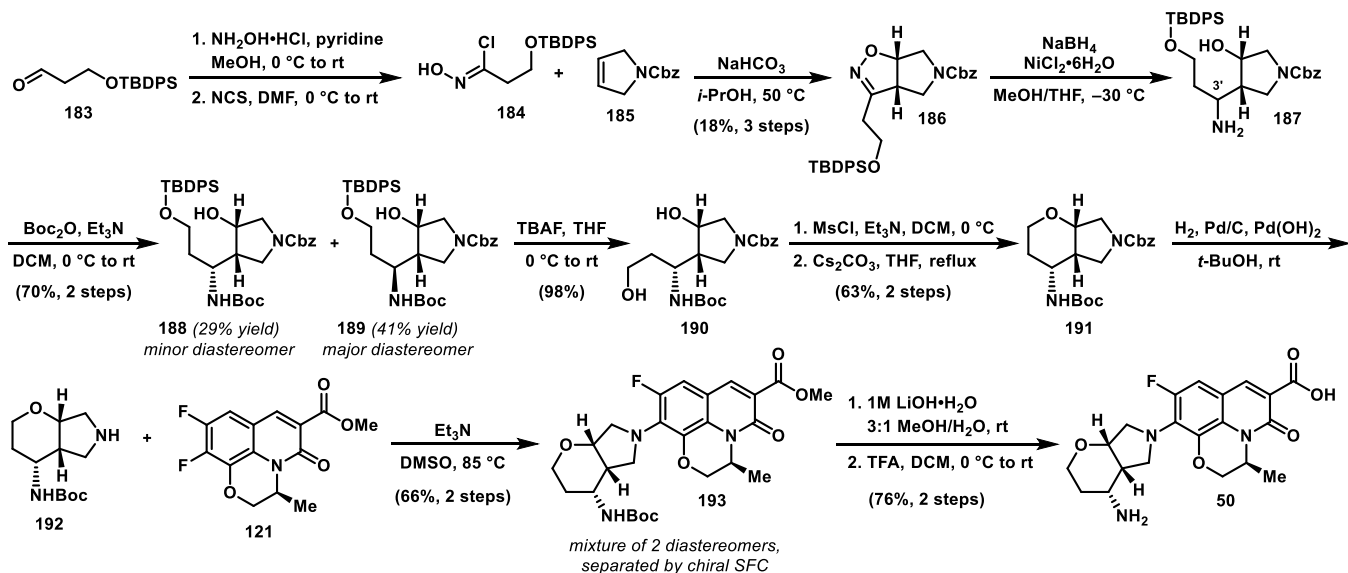
## Scheme 21. Synthesis of Compound 48



## Scheme 22. Synthesis of Compound 49



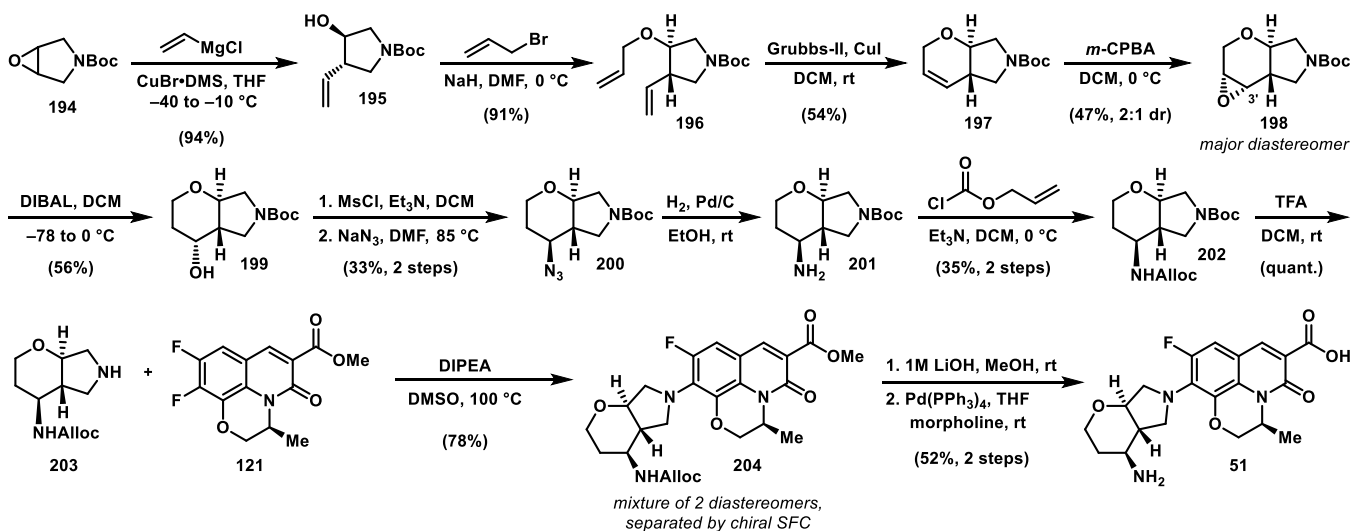
## Scheme 23. Synthesis of Compound 50



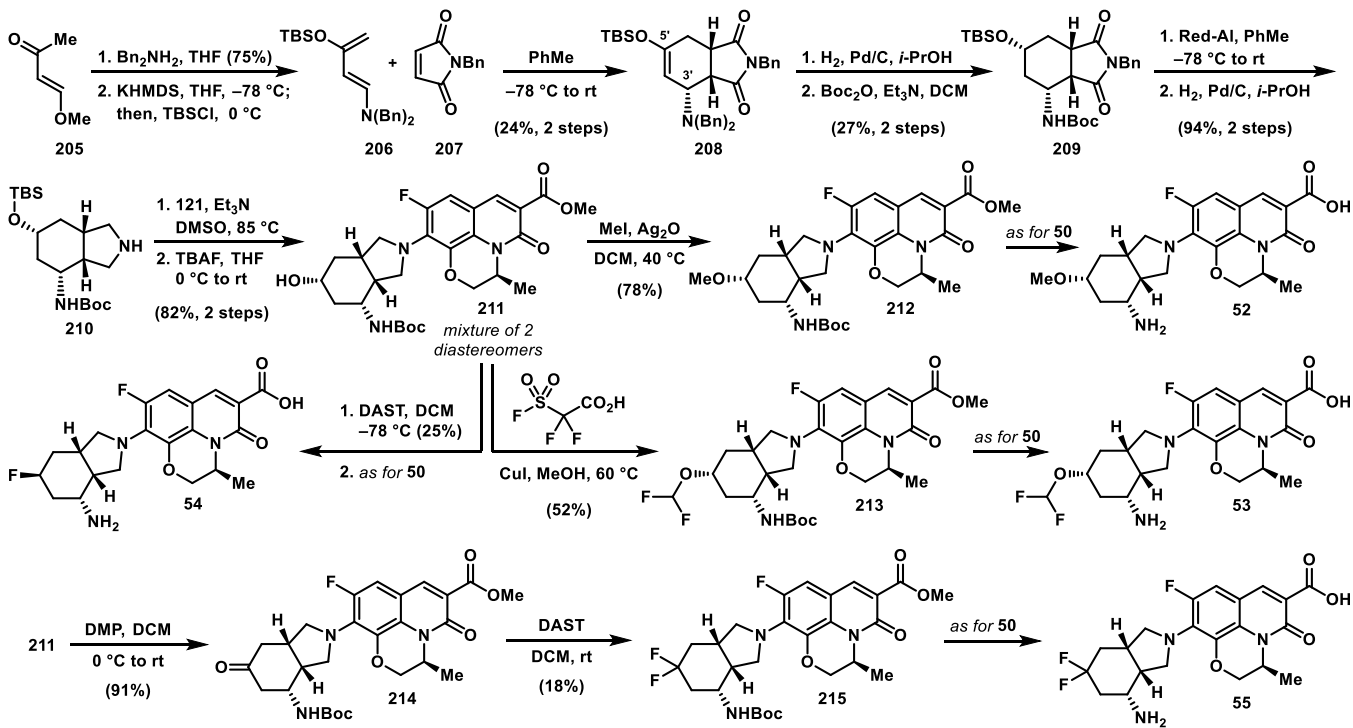
emerge from the 20th century's golden age of discovery. Identification of small-molecule inhibitors of their target enzymes, DNA gyrase and topoisomerase IV, which can overcome resistance to quinolones therefore represents a

promising avenue for drug discovery. By applying a scaffold morphing approach, we have documented the development of a unique series of antibacterial agents that combine elements of both quinazolinone and fluoroquinolone antibiotics. Early

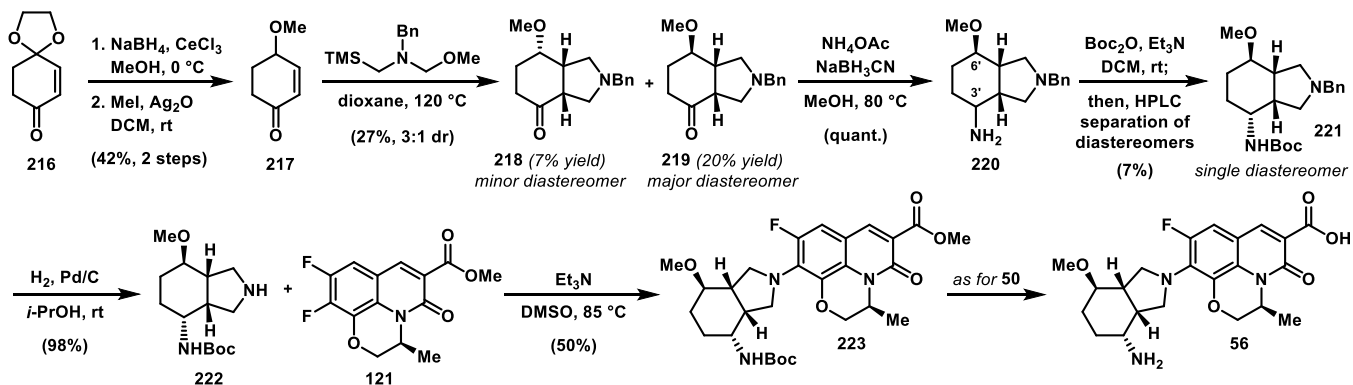
## Scheme 24. Synthesis of Compound 51



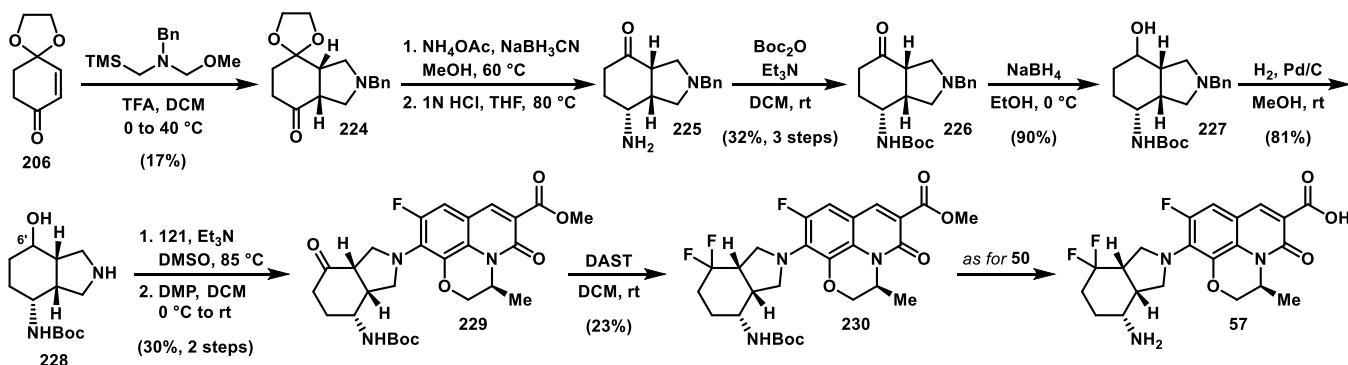
## Scheme 25. Synthesis of Compound 52–55



## Scheme 26. Synthesis of Compound 56



Scheme 27. Synthesis of Compound 57

Table 12. Bacterial Strains Used for *In Vitro* Experiments

Novartis strain code	referred to as	description	source or reference
NB01006	<i>S. aureus</i> FQ-S	ATCC 49951	ATCC
NB01006-AVR0005	<i>S. aureus</i> FQ-R	resistant mutant of ATCC 49951 selected on ciprofloxacin	this study
NB01080	<i>S. aureus</i> FQ-R clinical isolate	multidrug-resistant MRSA clinical isolate	JMI Laboratories
NB04001	<i>E. faecalis</i> FQ-S	ATCC 29212	ATCC
NB01007	<i>S. pneumoniae</i> FQ-S	ATCC 49619	ATCC

lead compounds such as 7 and 8 showed good activity against both FQ-S and FQ-R *S. aureus* and set the stage for investigation of compounds with more drastic modifications to the substituents at the C3 and C4 positions of the scaffold (see Tables 2 and 3). Compounds in this series were devoid of both the C3 carboxylate and C4 carbonyl that characterize classical quinolones and thus provided a unique platform to investigate SAR in a region of the quinolone binding pocket that has remained largely underexplored after decades of research. While a number of analogues exhibited good antibacterial activity, it proved challenging to identify compounds with appropriate *in vitro* safety and/or PK properties. Ultimately, merging features of (–)-8 with levofloxacin resulted in 25, a compound with an excellent overall profile including good antibacterial activity, low *in vitro* hERG inhibition, and good ADME properties. Optimization of the C7 substituent led to the discovery of a series of 5,6-fused bicyclic amines that provided enhanced antibacterial potency without sacrificing *in vitro* safety or PK properties (e.g., compound 55).

An X-ray co-crystal structure of 25 bound to a *K. pneumoniae* topoisomerase cleavage complex provided clarity on the binding mode and highlighted key differences with quinolones such as levofloxacin. In this structure, compound 25 does not engage in direct or water–metal ion bridge-mediated interactions with residues in the QRDR of *K. pneumoniae* topoisomerase IV. This binding mode suggests a rationale for the reduced impact of QRDR mutations in DNA gyrase and topoisomerase IV on the antibacterial activity of compound 25 compared to classical fluoroquinolones. The favorable PK profile of 25 translated into remarkable *in vivo* efficacy at doses lower than those required for moxifloxacin, even though the latter compound exhibits greater *in vitro* potency. These results demonstrate that bacterial DNA gyrase and topoisomerase IV continue to represent highly valuable targets for the discovery of novel antibiotics. Further profiling of 25 will be reported in due course.

## EXPERIMENTAL SECTION

All key compounds possessed a purity of at least 95%, as assessed by analytical reversed phase HPLC (see the Supporting Information for details). For MIC data, the most frequently occurring value from three or more replicates is reported. In cases where two values occurred with identical frequency, the higher of the two values is reported. MIC data for the following compounds is the result of a single replicate: 6, 7, 10, 12–19, 23, 26–28, 31–33, 36–40, 42–47, 51, and 56.

**Antibacterial Susceptibility Testing.** Antibacterial activity was determined by broth microdilution assay following the recommended CLSI methodology (CLSI document M07)<sup>97</sup> against strains of *S. aureus*, *E. faecalis*, and *S. pneumoniae* (Tables 12 and 13).

Table 13. Bacterial Strains Used for *In Vivo* Studies (See Table 11)

Novartis strain code	referred to as	description	source or reference
NB01001	<i>S. aureus</i> FQ-S	ATCC 29213	ATCC
NB01058	<i>S. aureus</i> FQ-R clinical isolate	MRSA clinical isolate	AKH Vienna, Austria

**Protein X-ray Crystallography Studies.** Cloning, expression, and purification of the *K. pneumoniae* topoisomerase IV ParE–ParC fusion protein was published previously.<sup>19,33</sup> In brief, the ParE–ParC fusion gene was made by fusing the C-terminal domain of *parE* (residues 390–631) and the N-terminal domain of *parC* (residues 1–490) linked by a 2-amino acid Glu–Phe linker and followed by a C-terminal 6×-histidine tag. The ParEC fusion protein (MW ~ 84 kDa) was purified and concentrated to 7.6 mg/mL in 20 mM Tris pH 7.5, 100 mM NaCl, and 2 mM TCEP and stored at –80 °C for up to 6 months. HPLC purified DNA oligos, 5'-TTACGTTGTAT-3' and 5'-GATCATAACAACGTAA-3', were ordered from IDT and each dissolved in 10 mM Tris-HCl pH 7.5 and 50 mM NaCl to form a 2 mM solution. Equal volumes of each oligo were mixed and annealed by denaturing at 95 °C, followed by slow cooling to room temperature in a thermos flask over 48 h to form a 0.5 mM solution of symmetric doubly nicked duplex DNA. The protein–DNA–compound ternary complex was formed by mixing 23 μM (3.8 mg/mL) ParEC dimer, 34.5 μM symmetric doubly nicked duplex DNA, and 0.2 mM compound 25 in protein storage buffer supplemented with 10 mM MgCl<sub>2</sub>. Crystals of the complex were grown by mixing

ternary complex solution with crystallization solution (20% 2-methyl-2,4-pentanediol (MPD), 10 mM MgCl<sub>2</sub>, 0.5 mM spermine, 100 mM sodium cacodylate, pH 6.6) using a 2:1 drop ratio and crystals appeared within 24–48 h at 17 °C. Crystals were frozen in liquid nitrogen directly from the drop. Diffraction data were collected at the IMCA-CAT beamline at the Advanced Photon Source and processed with XDS. The structure was solved by molecular replacement using PDB 6WAA as starting model using Phaser.<sup>98</sup> The model was improved to convergence by iterative rounds of model rebuilding in Coot<sup>99,100</sup> and refinement using phenix.refine of the Phenix suite.<sup>101,102</sup>

**Small-Molecule X-ray Crystallography Studies.** *Crystallization.* Crystals suitable for diffraction experiments were obtained from amorphous materials by slow evaporation of the solvent mixtures given in Tables S2–S8.

*Data Collection.* Intensity data were collected at 100 K on a Bruker AXS three-circle diffractometer with monochromated Cu K $\alpha$  radiation, microfocus rotating anode generator, and a Smart 6000 charge-coupled device detector. Data processing and global cell refinement were performed with Saint. A semiempirical absorption correction was applied based on the intensities of symmetry-related reflections measured at different angular settings (SADABS). Crystal data, data collection parameters, and convergence results are listed in Tables S2–S8.

*Structure Solution and Refinement.* All structures were solved by dual space-recycling methods and subsequent difference Fourier (DF) syntheses and refined based on full-matrix least-squares on  $F_2$ . Anisotropic displacement parameters were used for all nonhydrogen atoms. Hydrogen atoms were located in DF maps and refined in idealized positions using a riding model. **24** crystallizes with one equivalent of water, and the chloride ion is disordered over two positions (ratio 0.85:0.15). **25** crystallizes with two independent molecules in the asymmetric unit. **48** crystallizes with 1 equivalent of water and 1 equivalent of methanol. **49** contains a cavity of approximately 346 Å<sup>3</sup>, located at (0,0,1/2) and filled with disordered solvent, presumably the solvent of crystallization, ethanol. The contribution of the disordered solvent to the scattering factors was taken into account with PLATON/SQUEEZE.<sup>103</sup> A total of 114 electrons were found in the cavity, corresponding to approximately six molecules of ethanol. Where relevant, the crystal data reported in Table S5 are given without the contribution of the disordered solvent. **50** crystallizes with four equivalents of water. **52** crystallizes with one equivalent of water, and the OMe group is disordered over two positions (ratio 0.69:0.31). Additionally, there is a cavity of approximately 154 Å<sup>3</sup>, located at (0,0,1/2) and filled with disordered solvent, presumably the solvent of crystallization, ethanol. The contribution of the disordered solvent to the scattering factors was taken into account with PLATON/SQUEEZE.<sup>103</sup> A total of 38 electrons was found in the cavity, corresponding to approximately two molecules of ethanol. Where relevant, the crystal data reported in Table S7 are given without the contribution of the disordered solvent. **54** crystallizes with two independent molecules in the asymmetric unit, which also contains three water molecules and one isopropanol. Hydrogen atoms at the water molecules could not be located in the DF maps. The chloride ion is disordered over two positions (ratio 0.84:0.16).

Crystallographic data (excluding structure factors) have been deposited with the Cambridge Crystallographic Data Centre as supplementary publication numbers CCDC 2059545 (**24**), CCDC 2059541 (**25**), CCDC 2059546 (**48**), CCDC 2059544 (**49**), CCDC 2059547 (**50**), CCDC 2059542 (**52**), and CCDC 2059543 (**54**). Copies of the data can be obtained free of charge on application to CCDC, 12 Union Road, Cambridge CB2 1EZ, UK. Email: [deposit@ccdc.cam.ac.uk](mailto:deposit@ccdc.cam.ac.uk).

**In Vivo PK Studies.** All animal studies were conducted under a Novartis-Emeryville IACUC-approved protocol in compliance with Animal Welfare Act regulations and the Guide for the Care and Use of Laboratory Animals. Animals were fasted overnight and dosed IV and PO at the targeted doses in a solution of the indicated vehicle (see Tables 4 and 10). The whole blood was collected into vials containing

ethylenediaminetetraacetic acid at postdose 0.083, 0.25, 0.5, 1, 2, 4, 6, 8, and 24 h and immediately placed on dry ice until all samples were stored in a –80 °C freezer. Prior to analysis, the samples were thawed on ice. Ten microliters of each blood sample were added to 80  $\mu$ L of acetonitrile containing internal standard (IS) (CHIRO73911) and centrifuged 3450g at 10 °C for 20 min. A 70  $\mu$ L aliquot of the supernatant was transferred into a microtiter plate and dried down at 40 °C, and the residue was reconstituted with 100  $\mu$ L of 0.1% formic acid (FA) in water. An aliquot of each sample was injected into the liquid chromatography/mass spectrometry/mass spectrometry (LC–MS/MS) system for analysis. Noncompartmental PK analysis was conducted using Phoenix WinNonlin 6.4 professional (6.4) (Certara, Inc., Menlo Park, CA) to generate pharmacokinetic parameters.

**Animal Infection Models.** All animal experiments were approved by and conducted in accordance with the guidelines of the Institutional Animal Care and Use Committee of Novartis. Animals were maintained under controlled conditions with free access to food and water.

*Thigh Infection Model.* Mice were rendered neutropenic by two injections of cyclophosphamide (Sigma Chemical Co., St. Louis, MO) at doses of 150 mg/kg intraperitoneally (i.p.) and 100 mg/kg i.p. 4 and 1 day prior to infection, respectively. Animals were infected with either NB01001 or NB01058 with the inoculum prepared at  $2 \times 10^7$  cfu/mL from an overnight culture. High infections were established by intramuscular injection of 50  $\mu$ L of the bacterial suspension into the left hind thigh of female CD1 mice (Envigo,  $n = 4$ , 20–25 g). Novel compounds were formulated in PEG/Solutol/DSW and administered 2 h post infection *via* the subcutaneous route at doses ranging from 6.25 to 120 mg/kg. Standard antibiotic moxifloxacin was formulated in deionized water. All compounds were administered as hydrochloride salts with the exception of compound **55**, which was administered as a trifluoroacetate salt. Control mice were treated with the vehicle only. Twenty-four hours after start of treatment, the mice were euthanized and the thighs aseptically excised. Thigh muscles were homogenized in 5 mL of saline, and appropriate dilutions were plated onto blood agar plates to determine the number of viable bacteria per thigh. The static dose (mg/kg/day) is the dose of drug which maintains the level of bacteria at the start of treatment (0 h). Dose/day was plotted against log<sub>10</sub> cfu and analyzed using a four parametric logistic curve (SigmaPlot 12.0, SyStat Software, San Jose, California). The static dose was calculated using the following equation:  $\log_{10} \text{ static dose} = \{\log_{10}[E/(E_{\text{max}} - E)]/N\} + \log_{10} \text{ED}_{50}$ , where  $E$  is the control growth (log<sub>10</sub> change in cfu per thigh in untreated controls after the 24 h period of study),  $E_{\text{max}}$  is the maximum effect,  $\text{ED}_{50}$  is the dose required to achieve 50% of  $E_{\text{max}}$ , and  $N$  is the slope of the dose effect curve.  $E + 1$  and  $E + 2$  were used to calculate 1-log kill effect and 2-log kill effect, respectively.

**Additional In Vitro Assays. Log D<sub>7,4</sub> Determination.** A total of 10  $\mu$ L of compound stock solutions [10 mM in dimethyl sulfoxide (DMSO)] was placed in each well of a 96-well plate. A total of 5  $\mu$ L of 2 mM halodipine (log  $D = 3.00$ ) was added to each well as an IS and mixed. DMSO was removed using a lyophilizer (overnight). A total of 250  $\mu$ L of water [phosphate-buffered saline (PBS), pH = 7.4]–saturated octanol was added to each well, followed by 250  $\mu$ L of octanol–saturated water (PBS, pH = 7.4), and the plate was vortexed overnight. A total of 100  $\mu$ L of the octanol phase was removed from each well, diluted 1:100 with DMSO, and 1  $\mu$ L was injected into a LC/UV/quadrupole time-of-flight (qTOF) system [reverse-phase (RP) column]. A total of 100  $\mu$ L of the water phase was removed from each well, and 10  $\mu$ L was injected into the LC/UV/qTOF system (RP column). Data was processed with ProfileLynx. Mass chromatograms were integrated, corrected for dilution and injection volumes, and, finally, corrected using the area ratio of IS. IS peak areas were adjusted to fit the theoretical concentration for aqueous and octanol phases for the known log  $D$  value.

Log  $D$  was calculated according to the following

$$\text{analyte log } D = \log(\text{ratio}_{\text{oct}}/\text{ratio}_{\text{aq}})$$

$$\text{ratio}_{\text{oct}} = (\text{undiluted analyte}_{\text{peak area}}/\text{adjusted IS}_{\text{peak area}})_{\text{oct}}$$

$$\text{ratio}_{\text{aq}} = (\text{undiluted analyte}_{\text{peak area}}/\text{adjusted IS}_{\text{peak area}})_{\text{aq}}$$

**Solubility Determination.** A total of 20  $\mu\text{L}$  of 10 mM DMSO compound stock solution was transferred into a 96-deep-well “sample plate”. A total of 5  $\mu\text{L}$  of 10 mM DMSO stock solution was transferred to a second “compound standard plate”. The sample plate was placed in a Multi-Tainer MT-4 container (FTS Systems) and freeze-dried overnight to remove DMSO. 100  $\mu\text{L}$  of PBS (pH 7.0) was added to the dried compound in the sample plate and 95  $\mu\text{L}$  of DMSO to the standard plate. The sample plate was sonicated in a water bath for 10 min. The two plates were then placed onto a VWR orbital shaker to equilibrate for 24 h at room temperature and then centrifuged at 4000 rpm for 30 min. Then, 10  $\mu\text{L}$  aliquots of supernatant from the sample plate were removed and diluted 5-fold. Compound standard and sample were injected into an ultra-performance LC/UV/CLND/MS system to generate multi detector qualitative and quantitative analytical data. Data were processed with Xcalibur. CLND equimolar response was used for measuring compound concentration of DMSO solution and UV 270 nm or MS relative ratio for was used for solubility determination.

**$pK_a$  Measurements.**  $pK_a$  values were determined using either the UV-metric or potentiometric method as described previously.<sup>104</sup> UV metric method: UV-metric ionization constants were determined on the commercial spectral gradient analyzer or T3 instrument (Sirius Analytical Ltd., [sirius-analytical.com](http://sirius-analytical.com)), as described by Allen *et al.*<sup>105</sup> Test compounds were diluted to 0.04 mM in a cosolvent mixture and titrated three times in 20–40% wt methanol. The titrations were performed at 25 °C and 0.15 M ionic strength, from pH 2 to 12 or 12 to 2 (with a delta pH of 0.2) depending on the acidic or basic nature of the test compound. A linear buffer was added to allow fast pH stabilization after each titrant addition. Wavelengths from 230 to 450 nm were typically monitored for UV absorbance change due to the ionization state of the compound. Target factor analysis was used to calculate apparent  $pK_a$ 's from the multiwavelength absorption data at a given percent of cosolvent ( $psK_a$ ), followed by Yasuda–Shedlovsky extrapolation to 0% methanol to provide the aqueous  $pK_a$ . Acid/base assignment was performed based on the slope of extrapolation. Potentiometric method: potentiometric ionization constants were determined on the commercial GpKa or T3 instruments (Sirius Analytical) as described by Takács-Novák *et al.*<sup>106</sup> In brief, 0.3–1 mM test solutions were titrated from pH 2 to 12 or 12 to 2, depending on the acidic or basic nature of the test compound. Titrations were conducted at 25 °C and 0.15 M ionic strength. Aqueous titrations were performed in triplicate in 0.15 M KCl, while sparingly soluble test compounds were titrated in 10–60% wt methanol, 1,4-dioxane, or DMSO cosolvent. A minimum of three titrations in varying amounts of the cosolvent were performed for Yasuda–Shedlovsky extrapolation to the aqueous  $pK_a$ . For each titration, initial estimates of  $pK_a$  values were obtained from Bjerrum difference plots (number of bound protons *vs* pH) and further refined by a weighted nonlinear least-squares procedure (see Avdeef<sup>107,108</sup>) available in the instrument software.

**In Vitro Plasma Protein Binding.** Compounds were spiked into plasma of selected species (male CD-1 mouse, male Sprague Dawley rat or pooled human plasma, all in lithium heparin preparations, BioreclamationIVT) in the “plasma chamber” of a rapid equilibrium device (Thermo Scientific) plate at a final concentration of 10  $\mu\text{M}$  (1% DMSO in the incubation) and allowed to reach equilibrium between the “plasma chamber” and “buffer chamber” (100 mM PBS) for 4 h in a shaking incubator (37 °C, 800 rpm). Compounds were tested in duplicate. At the end of incubation, samples were collected from plasma and buffer chambers, followed by bioanalysis using LC–MS/MS. The percent plasma protein binding of a test compound was estimated using the following equation

$$\text{PPB} (\%) = 100 \times (1 - C_{\text{buffer}}/C_{\text{plasma}})$$

where  $C_{\text{buffer}}$  and  $C_{\text{plasma}}$  are compound concentrations in the buffer and plasma chambers at equilibrium, respectively.

Recovery of a compound after the incubation was also calculated as % recovery

$$\text{recovery} (\%) = 100 \times (C_{\text{buffer}} \times V_{\text{buffer}} + C_{\text{plasma}} \times V_{\text{plasma}}) / (C_0 \times V_{\text{plasma}})$$

where  $V_{\text{buffer}}$  and  $V_{\text{plasma}}$  are incubation volumes in buffer and plasma chambers, respectively.  $C_0$  is the initial compound concentration in plasma at the beginning of the incubation.

**Caco-2 Permeability.** Caco-2 cells were cultured for 21 days on 96-well transwell plates. Test compound solutions were prepared by diluting 7  $\mu\text{L}$  of 2 mM DMSO stock solution in transport buffer to a final volume of 1.4 mL (final compound concentration was 10  $\mu\text{M}$ ). Test compound solutions were transferred to either the apical or basolateral chambers of the 96-well transwell plates (the donor wells). Transport buffer was then added to the respective receiver wells. Plates were then incubated for 2 h at 37 °C with shaking/vortex. Donor wells were sampled at  $t = 0$ . Apical and basolateral wells were sampled at  $t = 2$  h. Samples were analyzed by LC–MS/MS. Transport from A–B and B–A was measured in triplicate. Apparent compound permeability is calculated as follows

$$P_{\text{app}} = (\partial Q/\partial t) \times (1/AC_0)$$

where  $\partial Q/\partial t$  is the total amount of compound transported to the recipient chamber per unit time (*e.g.*, nmol/s);  $A$  is the surface area of the transport membrane ( $\text{cm}^2$ ), and  $C_0$  is the initial compound concentration in the donor chamber (*e.g.*, nmol/mL).  $P_{\text{app}}$  is expressed as  $\text{cm/s}$ .

**hERG Radioligand Binding Assay (Conducted by Eurofins Scientific).** Cell membrane homogenates (about 40  $\mu\text{g}$  protein) were incubated for 60 min at 22 °C with 3 nM [ $^3\text{H}$ ]dofetilide in the absence or presence of the test compound in a buffer containing 50 mM Tris-HCl (pH 7.4), 10 mM KCl, and 1 mM  $\text{MgCl}_2$ . Nonspecific binding was determined in the presence of 25  $\mu\text{M}$  terfenadine. Following incubation, the samples were filtered rapidly under vacuum through glass fiber filters (GF/B, Packard) presoaked with 0.3% polyethylenimine and rinsed several times with ice-cold 50 mM Tris-HCl, 10 mM KCl, and 1 mM  $\text{MgCl}_2$  using a 96-sample cell harvester (Unifilter, Packard). The filters were dried and then counted for radioactivity in a scintillation counter (Topcount, Packard) using a scintillation cocktail (MicroScint 0, Packard). Terfenadine was used as the standard reference compound.

**Automated Electrophysiology.** HEK293 cells stably transfected with  $\text{hNa}_v1.5$  channels were obtained from Millipore Corp. and grown in Dulbecco's modified Eagle medium (DMEM)/F-12 nutrient mixture supplemented with 10% fetal bovine serum (FBS), 1% nonessential amino acids, and neomycin (400 mg/mL, Invitrogen). Cells were cryopreserved in liquid nitrogen with 10% v/v DMSO and thawed immediately prior to the experiment. hERG and  $\text{hCa}_v1.2$  expressing cell lines were produced in-house at Novartis using the CHO-K1 T-REX inducible plasmid system (Invitrogen), as described previously.<sup>109</sup> Cell lines were maintained in Ham's F12 nutrient mixture containing 10% FBS, blasticidin (10 mg/mL; InvivoGen), hygromycin B (200 mg/mL; InvivoGen), Zeocin (200 mg/mL, Invitrogen), and neomycin (200 mg/mL, Invitrogen) using a Select automated cell culture system (TAP Biosystems, Cambridge, UK). hERG and  $\text{hCa}_v1.2$  channel expression was induced with tetracycline (0.25–1  $\mu\text{g}/\text{mL}$ , Invitrogen) at least 24 h prior to the experiment.

hERG currents were recorded using the QPatch automated patch clamp systems (Sophion Bioscience Inc., North Brunswick, NJ) in the whole (single) cell configuration. hERG expressing CHO-K1 cells were harvested with Detachin (Genlantis) and stored in the modified serum-free SFM-2 media (Life Technologies) at room temperature. The extracellular solution contained (in mM) NaCl (145), KCl (4),  $\text{MgCl}_2$  (1),  $\text{CaCl}_2$  (2), and 4-(2-hydroxyethyl)-1-piperazineethanesulfonic acid (HEPES) (10) at pH 7.4 with NaOH. The intracellular solution contained KCl (135),  $\text{MgCl}_2$  (1.75),  $\text{CaCl}_2$  (5.4), ethylene glycol tetraacetic acid (EGTA) (10), K2-adenosine 5'-triphosphate (4), and HEPES (10) at pH 7.2 with KOH. After whole cell configuration was achieved, the cell was held at  $-90$  mV, and a 0.1 s pulse to  $-50$  mV was delivered to measure the leaking current, which was subtracted from the tail current on-line. Then, the cell was



depolarized to +20 mV for 4 s (prepulse), followed by a 4 s test pulse to −50 mV to reveal the hERG tail current. To monitor changes in the current amplitude, this voltage protocol was repeatedly applied every 20 s. Test compounds were first diluted in DMSO for six dose–response experiments and then dissolved in the extracellular solution using a Freedom EVO liquid handling robotic system (Tecan, Männedorf, Switzerland). The final DMSO concentration in samples was 0.3% v/v. Amitriptyline (Sigma) was tested as a positive control. Data were analyzed using an in-house developed MatLab-based program (MathWorks, Natick, MA).

hERG QPatch testing for compound **48** was performed using a long incubation protocol (10 min per concentration point). To avoid current rundown during prolonged incubation, current was measured in duplicate ([11 and 100  $\mu$ M] and [33 and 300  $\mu$ M] concentration pairs) in different cells simultaneously. The results of these measurements were combined into one dose response-plot. Data were analyzed manually using Sophion QPatch Assay software.

$hNa_v1.5$  and  $hCa_v1.2$  currents were recorded using the IonWorks Quattro system (Molecular Devices LLC, San Jose, CA) in the population (64 cells/well) patch clamp mode. For the  $hNa_v1.5$  Quattro assay, the extracellular solution contained NaCl (137), KCl (4),  $MgCl_2$  (1),  $CaCl_2$  (1.8), HEPES (10), and glucose (10) at pH 7.3 with NaOH, and the intracellular solution contained potassium gluconate (100), KCl (40),  $MgCl_2$  (1), EGTA (1), and HEPES (10) at pH 7.2 with KOH. For the  $hCa_v1.2$  Quattro assay, the extracellular solution contained sodium gluconate (130), NaCl (20), KCl (5),  $MgCl_2$  (2),  $BaCl_2$  (10), HEPES (10), and glucose (5) at pH 7.3 with NaOH, and the intracellular solution contained potassium gluconate (100),  $MgCl_2$  (0.2), CsCl (40), EGTA (5), and HEPES (10) at pH 7.3 with CsOH. Amphotericin B (0.1 mg/mL, Sigma) was used to perforate the patch and gain electrical access to the cell. For the  $hNa_v1.5$  Quattro assay, the sodium currents were evoked by a train of 12 pulses from the holding potential of −90 to −20 mV at 5 Hz. In addition, 70 ms before each pulse, a 20 ms voltage pulse to −100 mV was applied for leak subtraction. For the  $hCa_v1.2$  Quattro assay, cells were clamped for 10 s at 90 mV, and then, calcium currents were evoked by a 100 ms depolarizing pulse to −10 mV applied once with the data sampling period of 0.1 ms. Then, a 40 ms hyperpolarizing pulse to −90 mV was applied before the main pulse for leak subtraction. Test compounds were first diluted in DMSO for seven dose–response experiments using Tecan Freedom EVO and then dissolved in the extracellular solution with a VIAFLO 384 electronic pipette (Integra Biosciences, Hudson, NH). Each compound plate contained 0.3% v/v DMSO vehicle control (for the current rundown estimation), amitriptyline (positive control for the  $hNa_v1.5$  Quattro assay), and nifedipine ( $hCa_v1.2$  Quattro assay). All experiments were performed at room temperature. Data were captured and analyzed using the Novartis in-house Helios application suite.

**Cytotoxicity Assay.** K562 (human leukemia cells) and HepG2 (human hepatocellular carcinoma cells) were used to determine compound cytotoxicity. Cell viability was quantified by using CellTiter-Glo, which measures ATP release based on the mono-oxygenation of luciferin catalyzed by  $Mg^{2+}$ , ATP, and molecular oxygen.

**Cell Line Maintenance Media.** K562 cells were maintained in Iscove's modification of DMEM supplemented with 1% penicillin/streptomycin and 10% heat-inactivated FBS. HepG2 cells were maintained in DMEM-F12 supplemented with 1% penicillin/streptomycin and 10% heat-inactivated FBS.

Cells were counted using a hemocytometer and diluted to  $2 \times 10^4$  cells/mL for K562 and  $5 \times 10^4$  cells/mL for HepG2 in the appropriate culture media. A total of 50  $\mu$ L of the cell suspension was added to each well of the 384-well assay plate containing 1  $\mu$ L of the serially diluted compound (100  $\mu$ M top concentration, 3.16 $\times$  dilution factor) using the BioTek MultiFlo-Stacker liquid dispenser. Plates were incubated 72 h at 37  $^\circ$ C, 5%  $CO_2$ , and 90% humidity. A total of 25  $\mu$ L of 1 $\times$  CellTiter-Glo was then added to each well of the assay plate. Plates were incubated for 10 min at room temperature before reading on the POLARstar-Omega plate reader using the Luminescence settings and a gain of 3300. The 50% cytotoxic

concentrations ( $CC_{50}$ ) were determined. When multiple  $CC_{50}$  were determined for the same compound, the average is reported. If one or more  $CC_{50}$  for the same compound showed a value >100  $\mu$ M (top concentration tested), 100  $\mu$ M was used as the value in the average calculation.

## ■ ASSOCIATED CONTENT

### Supporting Information

The Supporting Information is available free of charge at <https://pubs.acs.org/doi/10.1021/acs.jmedchem.1c00375>.

Molecular formula strings (CSV)

Crystallographic data table and associated figures for the structure of compound **25** bound to topoisomerase IV; small-molecule crystal structures and associated data tables for compounds **24**, **25**, **48**, **49**, **50**, **52**, and **54**; synthesis and characterization of all final compounds and intermediates; and LC–MS chromatograms for all final compounds (PDF)

### Accession Codes

Structural coordinates for **25** bound to *K. pneumoniae* topoisomerase IV have been deposited in the RCSB Protein Data Bank under the accession code 7LHZ. Crystallographic data for small molecules (excluding structure factors) have been deposited with the Cambridge Crystallographic Data Centre as supplementary publication numbers CCDC 2059545 (**24**), CCDC 2059541 (**25**), CCDC 2059546 (**48**), CCDC 2059544 (**49**), CCDC 2059547 (**50**), CCDC 2059542 (**52**), and CCDC 2059543 (**54**). Copies of the data can be obtained free of charge on application to the CCDC, 12 Union Road, Cambridge CB2 1EZ, UK. Email: [deposit@ccdc.cam.ac.uk](mailto:deposit@ccdc.cam.ac.uk). Authors will release the atomic coordinates upon article publication.

## ■ AUTHOR INFORMATION

### Corresponding Authors

Guillaume Lapointe – Novartis Institutes for BioMedical Research, Emeryville, California 94608, United States;

[orcid.org/0000-0002-0451-0505](https://orcid.org/0000-0002-0451-0505); Phone: +41 613245818; Email: [guillaume.lapointe@novartis.com](mailto:guillaume.lapointe@novartis.com)

Colin K. Skepper – Novartis Institutes for BioMedical Research, Emeryville, California 94608, United States;

[orcid.org/0000-0002-6771-2024](https://orcid.org/0000-0002-6771-2024); Phone: +1 510 879 9317; Email: [colin.skepper@novartis.com](mailto:colin.skepper@novartis.com)

### Authors

Lauren M. Holder – Novartis Institutes for BioMedical Research, Emeryville, California 94608, United States;

[orcid.org/0000-0001-8585-8169](https://orcid.org/0000-0001-8585-8169)

Duncan Armstrong – Novartis Institutes for BioMedical Research, Cambridge, Massachusetts 02139, United States

Cornelia Bellamacina – Novartis Institutes for BioMedical Research, Emeryville, California 94608, United States

Johanne Blais – Novartis Institutes for BioMedical Research, Emeryville, California 94608, United States

Dirksen Bussiere – Novartis Institutes for BioMedical Research, Emeryville, California 94608, United States;

[orcid.org/0000-0002-5623-5648](https://orcid.org/0000-0002-5623-5648)

Jianwei Bian – Novartis Global Drug Development, Shanghai 201203, China

Cody Cepura – Novartis Institutes for BioMedical Research, Emeryville, California 94608, United States

Helen Chan – Novartis Institutes for BioMedical Research, Emeryville, California 94608, United States

- Charles R. Dean** – Novartis Institutes for BioMedical Research, Emeryville, California 94608, United States
- Gianfranco De Pascale** – Novartis Institutes for BioMedical Research, Emeryville, California 94608, United States
- Bhavesh Dhumale** – Piramal Discovery Solutions, Ahmedabad, Gujarat 382213, India
- L. Mark Fisher** – Molecular and Clinical Sciences Research Institute, St George's, University of London, London SW17 0RE, U.K.; [orcid.org/0000-0002-2172-3369](https://orcid.org/0000-0002-2172-3369)
- Mangesh Fulsunder** – Piramal Discovery Solutions, Ahmedabad, Gujarat 382213, India
- Bhavin Kantariya** – Piramal Discovery Solutions, Ahmedabad, Gujarat 382213, India
- Julie Kim** – Novartis Institutes for BioMedical Research, Emeryville, California 94608, United States
- Sean King** – Novartis Institutes for BioMedical Research, Emeryville, California 94608, United States
- Lauren Kossy** – Novartis Institutes for BioMedical Research, Emeryville, California 94608, United States
- Upendra Kulkarni** – Novartis Institutes for BioMedical Research, Emeryville, California 94608, United States
- Jay Lakshman** – Novartis Global Drug Development, East Hanover, New Jersey 07936, United States
- Jennifer A. Leeds** – Novartis Institutes for BioMedical Research, Emeryville, California 94608, United States; [orcid.org/0000-0003-2244-4713](https://orcid.org/0000-0003-2244-4713)
- Xiaolan Ling** – Novartis Global Drug Development, Shanghai 201203, China
- Anatoli Lvov** – Novartis Institutes for BioMedical Research, Cambridge, Massachusetts 02139, United States
- Sylvia Ma** – Novartis Institutes for BioMedical Research, Emeryville, California 94608, United States
- Swapnil Malekar** – Novartis Institutes for BioMedical Research, Emeryville, California 94608, United States
- David McKenney** – Novartis Institutes for BioMedical Research, Emeryville, California 94608, United States
- Wosenu Mergo** – Novartis Institutes for BioMedical Research, Emeryville, California 94608, United States
- Louis Metzger** – Novartis Institutes for BioMedical Research, Emeryville, California 94608, United States
- Keshav Mhaske** – Piramal Discovery Solutions, Ahmedabad, Gujarat 382213, India
- Heinz E. Moser** – Novartis Institutes for BioMedical Research, Emeryville, California 94608, United States
- Mina Mostafavi** – Novartis Institutes for BioMedical Research, Emeryville, California 94608, United States
- Sunil Namballa** – Piramal Discovery Solutions, Ahmedabad, Gujarat 382213, India
- Jonas Noeske** – Novartis Institutes for BioMedical Research, Emeryville, California 94608, United States
- Colin Osborne** – Novartis Institutes for BioMedical Research, Emeryville, California 94608, United States
- Ashish Patel** – Piramal Discovery Solutions, Ahmedabad, Gujarat 382213, India
- Darshit Patel** – Piramal Discovery Solutions, Ahmedabad, Gujarat 382213, India
- Tushar Patel** – Piramal Discovery Solutions, Ahmedabad, Gujarat 382213, India
- Philippe Piechon** – Novartis Institutes for BioMedical Research, Basel 4002, Switzerland
- Valery Polyakov** – Novartis Institutes for BioMedical Research, Emeryville, California 94608, United States
- Krunal Prajapati** – Piramal Discovery Solutions, Ahmedabad, Gujarat 382213, India
- Katherine R. Prosen** – Novartis Institutes for BioMedical Research, Emeryville, California 94608, United States; [orcid.org/0000-0001-6301-8089](https://orcid.org/0000-0001-6301-8089)
- Folkert Reck** – Novartis Institutes for BioMedical Research, Emeryville, California 94608, United States; [orcid.org/0000-0001-7250-2526](https://orcid.org/0000-0001-7250-2526)
- Daryl L. Richie** – Novartis Institutes for BioMedical Research, Emeryville, California 94608, United States
- Mark R. Sanderson** – Randall Centre for Cell and Molecular Biophysics, King's College, London SE1 1UL, U.K.
- Shailesh Satasia** – Piramal Discovery Solutions, Ahmedabad, Gujarat 382213, India
- Bhautik Savani** – Piramal Discovery Solutions, Ahmedabad, Gujarat 382213, India
- Jogitha Selvarajah** – Molecular and Clinical Sciences Research Institute, St George's, University of London, London SW17 0RE, U.K.
- Vijay Sethuraman** – Novartis Institutes for BioMedical Research, Emeryville, California 94608, United States
- Wei Shu** – Novartis Institutes for BioMedical Research, Emeryville, California 94608, United States
- Kyuto Tashiro** – Novartis Institutes for BioMedical Research, Emeryville, California 94608, United States
- Katherine V. Thompson** – Novartis Institutes for BioMedical Research, Emeryville, California 94608, United States
- Krishniah Vaarla** – Piramal Discovery Solutions, Ahmedabad, Gujarat 382213, India
- Lakhan Vala** – Piramal Discovery Solutions, Ahmedabad, Gujarat 382213, India
- Dennis A. Veselkov** – Randall Centre for Cell and Molecular Biophysics, King's College, London SE1 1UL, U.K.
- Jason Vo** – Novartis Institutes for BioMedical Research, Emeryville, California 94608, United States
- Bhavesh Vora** – Piramal Discovery Solutions, Ahmedabad, Gujarat 382213, India
- Trixi Wagner** – Novartis Institutes for BioMedical Research, Basel 4002, Switzerland
- Laura Wedel** – Novartis Institutes for BioMedical Research, Emeryville, California 94608, United States
- Sarah L. Williams** – Novartis Institutes for BioMedical Research, Emeryville, California 94608, United States
- Satya Yendluri** – Novartis Institutes for BioMedical Research, Emeryville, California 94608, United States
- Qin Yue** – Novartis Institutes for BioMedical Research, Emeryville, California 94608, United States
- Areghaegn Yifru** – Novartis Institutes for BioMedical Research, Emeryville, California 94608, United States
- Yong Zhang** – Novartis Global Drug Development, Shanghai 201203, China
- Alexey Rivkin** – Novartis Institutes for BioMedical Research, Emeryville, California 94608, United States

Complete contact information is available at:  
<https://pubs.acs.org/10.1021/acs.jmedchem.1c00375>

#### Author Contributions

Alexey Rivkin was the Project Team Leader for this drug discovery program. The manuscript was written through contributions of all authors. All authors have given approval to the final version of the manuscript.

## Funding

This work was funded by the Novartis Institutes for BioMedical Research.

## Notes

The authors declare the following competing financial interest(s): Guillaume Lapointe, Colin K. Skepper, Lauren M. Holder, Duncan Armstrong, Cornelia Bellamacina, Johanne Blais, Dirksen Bussiere, Jianwei Bian, Cody Cepura, Helen Chan, Charles R. Dean, Gianfranco De Pascale, Julie Kim, Sean King, Lauren Kossy, Upendra Kulkarni, Jay Lakshman, Jennifer A. Leeds, Xiaolan Ling, Anatoli Lvov, Sylvia Ma, Swapnil Malekar, David McKenney, Wosenu Mergo, Louis Metzger, Heinz E. Moser, Mina Mostafavi, Jonas Noeske, Colin Osborne, Philippe Piechon, Valery Polyakov, Katherine R. Prosen, Folkert Reck, Daryl L. Richie, Vijay Sethuraman, Wei Shu, Kyuto Tashiro, Katherine V. Thompson, Jason Vo, Trixie Wagner, Laura Wedel, Sarah L. Williams, Satya Yendluri, Qin Yue, Aregahegn Yifru, Yong Zhang, and Alexey Rivkin are or were employees of Novartis.

## ACKNOWLEDGMENTS

The authors thank Shengtian Yang for NMR structure elucidation support; Weiping Jia, Heidi Struble, Dazhi Tang, and Alice Wan Wang for analytical and separations support; Linhong Yang for  $pK_a$  determination; Colin Lorentzen, Kent Wong, and Linda Xiao for *in vitro* ADME assays; and Michael Wang for synthesis of compound 6. The authors acknowledge Bellen Chemistry Co., Ltd. for scale up of compound 121. We thank AKH Vienna for strain NB01058 and JMI Laboratories for strain NB01080.

## ABBREVIATIONS

BA, bioavailability; BINAP, 2,2'-bis(diphenylphosphino)-1,1'-binaphthalene;  $C_{max}$ , maximum plasma concentration; CDI, carbonyl diimidazole; CL, clearance;  $CL_{int}$ , intrinsic clearance; DIPEA, *N,N*-diisopropylethylamine; DPPF, 1,1'-ferrocenediyl-bis(diphenylphosphine); FQ, fluoroquinolone; FQ-R, fluoroquinolone resistant; % *F*, percent orally bioavailable;  $fAUC$ , free (unbound) area under the curve; LiHMDS, lithium bis(trimethylsilyl)amide; MeCN, acetonitrile; NaHMDS, sodium bis(trimethylsilyl)amide; NT, not tested; QRDR, quinolone resistance determining region; TMAF, tetramethyl ammonium fluoride;  $T_{max}$ , time at which the maximum plasma concentration was reached;  $V_{ss}$ , volume of distribution

## REFERENCES

- (1) Mayer, C.; Janin, Y. L. Non-quinolone inhibitors of bacterial type IIA topoisomerases: a feat of bioisosterism. *Chem. Rev.* **2014**, *114*, 2313–2342.
- (2) Basarab, G. S. Four ways to skin a cat: inhibition of bacterial topoisomerases leading to the clinic. In *Topics in Medicinal Chemistry: Antibacterials*; Fisher, J. F., Mobashery, S., Miller, M. J., Eds.; Springer International Publishing: Cham, 2017; Vol. 25, pp 165–188.
- (3) Da Silva, A.; De Almeida, M.; De Souza, M.; Couri, M. Biological activity and synthetic methodologies for the preparation of fluoroquinolones, a class of potent antibacterial agents. *Curr. Med. Chem.* **2003**, *10*, 21–39.
- (4) Emmerson, A. M.; Jones, A. M. The quinolones: decades of development and use. *J. Antimicrob. Chemother.* **2003**, *51*, 13–20.
- (5) Mitscher, L. A. Bacterial topoisomerase inhibitors: quinolone and pyridone antibacterial agents. *Chem. Rev.* **2005**, *105*, 559–592.
- (6) Andriole, V. T. The quinolones: past, present, and future. *Clin. Infect. Dis.* **2005**, *41*, S113–S119.

- (7) Wagman, A. S.; Wentland, M. P. Quinolone antibacterial agents. In *Comprehensive Medicinal Chemistry II*; Taylor, J. B., Triggle, D. J., Eds.; Elsevier: Oxford, 2007; pp 567–596.

- (8) Jacoby, G. A.; Hooper, D. C. Review of the quinolone family. In *Antibiotic Discovery and Development*; Dougherty, T. J., Pucci, M. J., Eds.; Springer: Boston, MA, 2012; pp 119–146.

- (9) Naeem, A.; Badshah, S.; Muska, M.; Ahmad, N.; Khan, K. The current case of quinolones: synthetic approaches and antibacterial activity. *Molecules* **2016**, *21*, 268.

- (10) Biscacchi, G. S. Origins of the quinolone class of antibacterials: an expanded “discovery story”. *J. Med. Chem.* **2015**, *58*, 4874–4882.

- (11) Outpatient Antibiotic Prescriptions—United States. 2015, <https://www.cdc.gov/antibiotic-use/community/programs-measurement/state-local-activities/outpatient-antibiotic-prescriptions-US-2015.html> (accessed March 21, 2019).

- (12) Aldred, K. J.; Kerns, R. J.; Osheroff, N. Mechanism of quinolone action and resistance. *Biochemistry* **2014**, *53*, 1565–1574.

- (13) Hooper, D. C.; Jacoby, G. A. Topoisomerase inhibitors: fluoroquinolone mechanisms of action and resistance. *Cold Spring Harbor Perspect. Med.* **2016**, *6*, a025320.

- (14) Drlica, K.; Malik, M.; Kerns, R. J.; Zhao, X. Quinolone-mediated bacterial death. *Antimicrob. Agents Chemother.* **2008**, *52*, 385–392.

- (15) Drlica, K.; Hiasa, H.; Kerns, R.; Malik, M.; Mustae, A.; Zhao, X. Quinolones: action and resistance updated. *Curr. Top. Med. Chem.* **2009**, *9*, 981–998.

- (16) Laponogov, I.; Sohi, M. K.; Veselkov, D. A.; Pan, X.-S.; Sawhney, R.; Thompson, A. W.; McAuley, K. E.; Fisher, L. M.; Sanderson, M. R. Structural insight into the quinolone–DNA cleavage complex of type IIA topoisomerases. *Nat. Struct. Mol. Biol.* **2009**, *16*, 667.

- (17) Laponogov, I.; Pan, X.-S.; Veselkov, D. A.; McAuley, K. E.; Fisher, L. M.; Sanderson, M. R. Structural basis of gate-DNA breakage and resealing by type II topoisomerases. *PLoS One* **2010**, *5*, No. e11338.

- (18) Bax, B. D.; Chan, P. F.; Eggleston, D. S.; Fosberry, A.; Gentry, D. R.; Gorrec, F.; Giordano, I.; Hann, M. M.; Hennessy, A.; Hibbs, M.; Huang, J.; Jones, E.; Jones, J.; Brown, K. K.; Lewis, C. J.; May, E. W.; Saunders, M. R.; Singh, O.; Spitzfaden, C. E.; Shen, C.; Shillings, A.; Theobald, A. J.; Wohlkonig, A.; Pearson, N. D.; Gwynn, M. N. Type IIA topoisomerase inhibition by a new class of antibacterial agents. *Nature* **2010**, *466*, 935.

- (19) Veselkov, D. A.; Laponogov, I.; Pan, X.-S.; Selvarajah, J.; Skamrova, G. B.; Branstrom, A.; Narasimhan, J.; Prasad, J. V. N. V.; Fisher, L. M.; Sanderson, M. R. Structure of a quinolone-stabilized cleavage complex of topoisomerase IV from *Klebsiella pneumoniae* and comparison with a related *Streptococcus pneumoniae* complex. *Acta Crystallogr., Sect. D: Struct. Biol.* **2016**, *72*, 488–496.

- (20) Wohlkonig, A.; Chan, P. F.; Fosberry, A. P.; Homes, P.; Huang, J.; Kranz, M.; Leydon, V. R.; Miles, T. J.; Pearson, N. D.; Perera, R. L.; Shillings, A. J.; Gwynn, M. N.; Bax, B. D. Structural basis of quinolone inhibition of type IIA topoisomerases and target-mediated resistance. *Nat. Struct. Mol. Biol.* **2010**, *17*, 1152.

- (21) Aldred, K. J.; McPherson, S. A.; Wang, P.; Kerns, R. J.; Graves, D. E.; Turnbough, C. L.; Osheroff, N. Drug interactions with *Bacillus anthracis* topoisomerase IV: biochemical basis for quinolone action and resistance. *Biochemistry* **2012**, *51*, 370–381.

- (22) Aldred, K. J.; McPherson, S. A.; Turnbough, C. L., Jr.; Kerns, R. J.; Osheroff, N. Topoisomerase IV-quinolone interactions are mediated through a water-metal ion bridge: mechanistic basis of quinolone resistance. *Nucleic Acids Res.* **2013**, *41*, 4628–4639.

- (23) Aldred, K. J.; Breland, E. J.; Vlčková, V.; Strub, M.-P.; Neuman, K. C.; Kerns, R. J.; Osheroff, N. Role of the water-metal ion bridge in mediating interactions between quinolones and *Escherichia coli* topoisomerase IV. *Biochemistry* **2014**, *53*, 5558–5567.

- (24) Yoshida, H.; Bogaki, M.; Nakamura, M.; Nakamura, S. Quinolone resistance-determining region in the DNA gyrase *gyrA* gene of *Escherichia coli*. *Antimicrob. Agents Chemother.* **1990**, *34*, 1271–1272.

- (25) Tse-Dinh, Y.-C. Targeting bacterial topoisomerases: how to counter mechanisms of resistance. *Future Med. Chem.* **2016**, *8*, 1085–1100.
- (26) Tran, T. P.; Ellsworth, E. L.; Stier, M. A.; Domagala, J. M.; Hollis Showalter, H. D.; Gracheck, S. J.; Shapiro, M. A.; Joannides, T. E.; Singh, R. Synthesis and structural–activity relationships of 3-hydroxyquinazoline-2,4-dione antibacterial agents. *Bioorg. Med. Chem. Lett.* **2004**, *14*, 4405–4409.
- (27) Ellsworth, E. L.; Tran, T. P.; Hollis Showalter, H. D.; Sanchez, J. P.; Watson, B. M.; Stier, M. A.; Domagala, J. M.; Gracheck, S. J.; Joannides, E. T.; Shapiro, M. A.; Dunham, S. A.; Hanna, D. L.; Huband, M. D.; Gage, J. W.; Bronstein, J. C.; Liu, J. Y.; Nguyen, D. Q.; Singh, R. 3-aminoquinazolinones as a new class of antibacterial agents demonstrating excellent antibacterial activity against wild-type and multidrug resistant organisms. *J. Med. Chem.* **2006**, *49*, 6435–6438.
- (28) Tran, T. P.; Ellsworth, E. L.; Sanchez, J. P.; Watson, B. M.; Stier, M. A.; Showalter, H. D. H.; Domagala, J. M.; Shapiro, M. A.; Joannides, E. T.; Gracheck, S. J.; Nguyen, D. Q.; Bird, P.; Yip, J.; Sharadendu, A.; Ha, C.; Ramezani, S.; Wu, X.; Singh, R. Structure-activity relationships of 3-aminoquinazolinones, a new class of bacterial type-2 topoisomerase (DNA gyrase and topo IV) inhibitors. *Bioorg. Med. Chem. Lett.* **2007**, *17*, 1312–1320.
- (29) Pan, X.-S.; Gould, K. A.; Fisher, L. M. Probing the differential interactions of quinazolinone PD 0305970 and quinolones with gyrase and topoisomerase IV. *Antimicrob. Agents Chemother.* **2009**, *53*, 3822–3831.
- (30) Aldred, K. J.; Schwanz, H. A.; Li, G.; McPherson, S. A.; Turnbough, C. L., Jr.; Kerns, R. J.; Osherooff, N. Overcoming target-mediated quinolone resistance in topoisomerase IV by introducing metal-ion-independent drug-enzyme interactions. *ACS Chem. Biol.* **2013**, *8*, 2660–2668.
- (31) Jeannot, F.; Taillier, T.; Despeyroux, P.; Renard, S.; Rey, A.; Mourez, M.; Poeverlein, C.; Khichane, I.; Perrin, M.-A.; Versluys, S.; Stavenger, R. A.; Huang, J.; Germe, T.; Maxwell, A.; Cao, S.; Huseby, D. L.; Hughes, D.; Bacqué, E. Imidazopyrazinones (IPYs): non-quinolone bacterial topoisomerase inhibitors showing partial cross-resistance with quinolones. *J. Med. Chem.* **2018**, *61*, 3565–3581.
- (32) Germe, T.; Vörös, J.; Jeannot, F.; Taillier, T.; Stavenger, R. A.; Bacqué, E.; Maxwell, A.; Bax, B. D. A new class of antibacterials, the imidazopyrazinones, reveal structural transitions involved in DNA gyrase poisoning and mechanisms of resistance. *Nucleic Acids Res.* **2018**, *46*, 4114–4128.
- (33) Skepper, C. K.; Armstrong, D.; Balibar, C. J.; Bauer, D.; Bellamacina, C.; Benton, B. M.; Bussiere, D.; De Pascale, G.; De Vicente, J.; Dean, C. R.; Dhumale, B.; Fisher, L. M.; Fuller, J.; Fulsunder, M.; Holder, L. M.; Hu, C.; Kantariya, B.; Lapointe, G.; Leeds, J. A.; Li, X.; Lu, P.; Lvov, A.; Ma, S.; Madhavan, S.; Malekar, S.; McKenney, D.; Mergo, W.; Metzger, L.; Moser, H. E.; Mutnick, D.; Noeske, J.; Osborne, C.; Patel, A.; Patel, D.; Patel, T.; Prajapati, K.; Prosen, K. R.; Reck, F.; Richie, D. L.; Rico, A.; Sanderson, M. R.; Satsia, S.; Sawyer, W. S.; Selvarajah, J.; Shah, N.; Shanghavi, K.; Shu, W.; Thompson, K. V.; Traebert, M.; Vala, A.; Vala, L.; Veselkov, D. A.; Vo, J.; Wang, M.; Widya, M.; Williams, S. L.; Xu, Y.; Yue, Q.; Zang, R.; Zhou, B.; Rivkin, A. Topoisomerase inhibitors addressing fluoroquinolone resistance in Gram-negative bacteria. *J. Med. Chem.* **2020**, *63*, 7773–7816.
- (34) Antibiotic Resistance Threats in the United States. 2013, <http://www.cdc.gov/drugresistance/threat-report-2013/> (accessed March 20, 2019).
- (35) Antibiotic Resistance Threats in the United States. 2019, <https://www.cdc.gov/drugresistance/pdf/threats-report/2019-ar-threats-report-508.pdf> (accessed Dec 23, 2020).
- (36) Sader, H. S.; Flamm, R. K.; Mendes, R. E.; Farrell, D. J.; Jones, R. N. Antimicrobial activities of ceftaroline and comparator agents against bacterial organisms causing bacteremia in patients with skin and skin structure infections in U.S. medical centers, 2008 to 2014. *Antimicrob. Agents Chemother.* **2016**, *60*, 2558.
- (37) Flamm, R. K.; Mendes, R. E.; Hogan, P. A.; Streit, J. M.; Ross, J. E.; Jones, R. N. Linezolid surveillance results for the United States (LEADER surveillance program 2014). *Antimicrob. Agents Chemother.* **2016**, *60*, 2273.
- (38) Kang, J.; Wang, L.; Chen, X.-L.; Triggle, D. J.; Rampe, D. Interactions of a series of fluoroquinolone antibacterial drugs with the human cardiac K<sup>+</sup> channel HERG. *Mol. Pharmacol.* **2001**, *59*, 122–126.
- (39) Redfern, W.; Carlsson, L.; Davis, A.; Lynch, W.; Mackenzie, I.; Palethorpe, S.; Siegl, P.; Strang, I.; Sullivan, A.; Wallis, R. Relationships between preclinical cardiac electrophysiology, clinical QT interval prolongation and torsade de pointes for a broad range of drugs: evidence for a provisional safety margin in drug development. *Cardiovasc. Res.* **2003**, *58*, 32–45.
- (40) Culley, C. M.; Lacy, M. K.; Klutman, N.; Edwards, B. Moxifloxacin: clinical efficacy and safety. *Am. J. Health-Syst. Pharm.* **2001**, *58*, 379–388.
- (41) Darpo, B.; Nebout, T.; Sager, P. T. Clinical evaluation of QT/QTc prolongation and proarrhythmic potential for nonantiarrhythmic drugs: the international conference on harmonization of technical requirements for registration of pharmaceuticals for human use E14 guideline. *J. Clin. Pharmacol.* **2006**, *46*, 498–507.
- (42) Liu, H. H. Safety profile of the fluoroquinolones: Focus on Levofloxacin. *Drug Saf.* **2010**, *33*, 353–369.
- (43) Domagala, J. M.; Hagen, S. E. Structure-activity relationships of the quinolone antibacterials in the new millennium: some things change and some do not. In *Quinolone Antimicrobial Agents*, 3rd ed.; Hooper, D. C., Rubinstein, E., Eds.; ASM Press: Washington, D.C., 2003; pp 3–18.
- (44) Grant, E. B.; Foleno, B. D.; Goldschmidt, R.; Hilliard, J. J.; Lin, S.-C.; Morrow, B.; Paget, S. D.; Weidner-Wells, M. A.; Xu, X.; Xu, X.; Murray, W. V.; Bush, K.; Macielag, M. J. 7-(4-Alkylidenylpiperidinyl)-quinolone bacterial topoisomerase inhibitors. *Bioorg. Med. Chem. Lett.* **2014**, *24*, 5502–5506.
- (45) Ogata, M.; Matsumoto, H.; Shimizu, S.; Kida, S.; Nakai, H.; Motokawa, K.; Miwa, H.; Matsuura, S.; Yoshida, T. Synthesis and antibacterial activity of new 7-(aminoazabicycloalkanyl)-quinolonecarboxylic acids. *Eur. J. Med. Chem.* **1991**, *26*, 889–906.
- (46) Inagaki, H.; Takahashi, H.; Takemura, M. Synthesis and antibacterial activity of novel 6-fluoro-1-[(1R,2S)-2-fluorocyclopropan-1-yl]-4-oxoquinoline-3-carboxylic acids bearing cyclopropane-fused 2-amino-8-azabicyclo[4.3.0]nonan-8-yl substituents at the C-7 position. *Bioorg. Med. Chem. Lett.* **2004**, *14*, 5193–5198.
- (47) Compound **48** was tested in the hERG QPatch assay using a non-standard long incubation protocol (see [Experimental Section](#) for details). Under the standard conditions, steady state was not reached for some recordings. This can result in underestimation of the true IC<sub>50</sub>.
- (48) Guram, A. S.; Rennels, R. A.; Buchwald, S. L. A simple catalytic method for the conversion of aryl bromides to arylamines. *Angew. Chem., Int. Ed.* **1995**, *34*, 1348–1350.
- (49) Louie, J.; Hartwig, J. F. Palladium-catalyzed synthesis of arylamines from aryl halides. Mechanistic studies lead to coupling in the absence of tin reagents. *Tetrahedron Lett.* **1995**, *36*, 3609–3612.
- (50) Wolfe, J. P.; Wagaw, S.; Buchwald, S. L. An improved catalyst system for aromatic carbon–nitrogen bond formation: the possible involvement of bis(phosphine) palladium complexes as key intermediates. *J. Am. Chem. Soc.* **1996**, *118*, 7215–7216.
- (51) Guari, Y.; van Es, D. S.; Reek, J. N. H.; Kamer, P. C. J.; van Leeuwen, P. W. N. M. An efficient, palladium-catalyzed, amination of aryl bromides. *Tetrahedron Lett.* **1999**, *40*, 3789–3790.
- (52) Maiti, D.; Fors, B. P.; Henderson, J. L.; Nakamura, Y.; Buchwald, S. L. Palladium-catalyzed coupling of functionalized primary and secondary amines with aryl and heteroaryl halides: two ligands suffice in most cases. *Chem. Sci.* **2011**, *2*, 57–68.
- (53) Bruno, N. C.; Tudge, M. T.; Buchwald, S. L. Design and preparation of new palladium precatalysts for C–C and C–N cross-coupling reactions. *Chem. Sci.* **2013**, *4*, 916–920.

(54) Wolkenberg, S. E.; Boger, D. L. Total Synthesis of Anhydrolycorinone Utilizing Sequential Intramolecular Diels–Alder Reactions of a 1,3,4-Oxadiazole. *J. Org. Chem.* **2002**, *67*, 7361–7364.

(55) Compound **11** was derived from prior Buchwald–Hartwig coupling with (*R*)-**54**, unlike **10** or **13** which utilized the racemic amine.

(56) Montoir, D.; Tonnerre, A.; Duflos, M.; Bazin, M.-A. Differential functionalization of 1,6-naphthyridin-2(1H)-ones through sequential one-pot Suzuki–Miyaura cross-couplings. *Eur. J. Org. Chem.* **2014**, 1487–1495.

(57) Sonogashira, K.; Tohda, Y.; Hagihara, N. A convenient synthesis of acetylenes: catalytic substitutions of acetylenic hydrogen with bromoalkenes, iodoarenes and bromopyridines. *Tetrahedron Lett.* **1975**, *16*, 4467–4470.

(58) Sonogashira, K. Palladium-catalyzed alkynylation: Sonogashira alkyne synthesis. In *Handbook of Organopalladium Chemistry for Organic Synthesis*; Negishi, E., Ed.; John Wiley and Sons, Inc., 2003; pp 493–529.

(59) Sobenina, L. N.; Tomilin, D. N.; Gotsko, M. D.; Ushakov, I. A.; Mikhaleva, A. I.; Trofimov, B. A. From 4,5,6,7-tetrahydroindoles to 3- or 5-(4,5,6,7-tetrahydroindol-2-yl)isoxazoles in two steps: a regioselective switch between 3- and 5-isomers. *Tetrahedron* **2014**, *70*, 5168–5174.

(60) Tschaen, D. M.; Desmond, R.; King, A. O.; Fortin, M. C.; Pipik, B.; King, S.; Verhoeven, T. R. An improved procedure for aromatic cyanation. *Synth. Commun.* **1994**, *24*, 887–890.

(61) Kaiser, N.-F. K.; Hallberg, A.; Larhed, M. In situ generation of carbon monoxide from solid molybdenum hexacarbonyl. A convenient and fast route to palladium-catalyzed carbonylation reactions. *J. Comb. Chem.* **2002**, *4*, 109–111.

(62) Stille, J. K. The palladium-catalyzed cross-coupling reactions of organotin reagents with organic electrophiles [new synthetic methods (58)]. *Angew. Chem., Int. Ed.* **1986**, *25*, 508–524.

(63) Kosugi, M.; Fugami, K. Overview of the Stille protocol with Sn. In *Handbook of Organopalladium Chemistry for Organic Synthesis*; Negishi, E., Ed.; John Wiley & Sons, Inc., 2003; Vol. 1.

(64) Yamanaka, H.; Sakamoto, T.; Kondo, Y.; Yasuharu, A. Reaction of aryl halides with (*Z*)-1-ethoxy-2-tributylstannylethene: a versatile method for the introduction of 2-ethoxyethyl group into aromatic nuclei. *Heterocycles* **1990**, *31*, 219.

(65) Lindgren, B. O.; Nilsson, T.; Husebye, S.; Mikalsen, Ø.; Leander, K.; Swahn, C.-G. Preparation of carboxylic acids from aldehydes (including hydroxylated benzaldehydes) by oxidation with chlorite. *Acta Chem. Scand.* **1973**, *27*, 888–890.

(66) Kraus, G. A.; Taschner, M. J. Model studies for the synthesis of quassinoids. 1. Construction of the BCE ring system. *J. Org. Chem.* **1980**, *45*, 1175–1176.

(67) Kraus, G. A.; Roth, B. Synthetic studies toward verrucarol. 2. Synthesis of the AB ring system. *J. Org. Chem.* **1980**, *45*, 4825–4830.

(68) Bal, B. S.; Childers, W. E.; Pinnick, H. W. Oxidation of  $\alpha,\beta$ -unsaturated aldehydes. *Tetrahedron* **1981**, *37*, 2091–2096.

(69) Brooks, D. W.; Lu, L. D.-L.; Masamune, S. C-acylation under virtually neutral conditions. *Angew. Chem., Int. Ed.* **1979**, *18*, 72–74.

(70) Jacobsen, N.; Kolind-Andersen, H.; Christensen, J. Synthesis of 3-isoxazolols revisited. Diketene and  $\beta$ -ketoesters as starting materials. *Can. J. Chem.* **1984**, *62*, 1940–1944.

(71) Suzuki, A. Overview of the Suzuki protocol with B. In *Handbook of Organopalladium Chemistry for Organic Synthesis*; Negishi, E., Ed.; John Wiley & Sons: New York, 2003; pp 249–262.

(72) Miyaura, N. Metal-catalyzed cross-coupling reactions of organoboron compounds with organic halides. In *Metal-Catalyzed Cross-Coupling Reactions*, 2nd ed.; de Meijere, A., Diederich, F., Eds.; Wiley-VCH: Weinheim, 2004; pp 41–123.

(73) Soli, E. D.; Manoso, A. S.; Patterson, M. C.; DeShong, P.; Favor, D. A.; Hirschmann, R.; Smith, A. B. Azide and cyanide displacements via hypervalent silicate intermediates. *J. Org. Chem.* **1999**, *64*, 3171–3177.

(74) Kohara, Y.; Kubo, K.; Imamiya, E.; Wada, T.; Inada, Y.; Naka, T. Synthesis and angiotensin II receptor antagonistic activities of

benzimidazole derivatives bearing acidic heterocycles as novel tetrazole bioisosteres. *J. Med. Chem.* **1996**, *39*, 5228–5235.

(75) Bacon, R. G. R.; Wright, J. R. Metal ions and complexes in organic reactions. Part X. Effect of methoxy-substituents on copper-catalysed nucleophilic and reductive replacement of halogen in reactions between sodium methoxide and bromo- or iodo-benzene derivatives. *J. Chem. Soc. C* **1969**, *15*, 1978–1981.

(76) Heaney, H.; Millar, I. T. Triphenylene. *Org. Synth.* **1960**, *40*, 105.

(77) Clive, D.; Angoh, A. G.; Bennett, S. M. Radical spirocyclization: synthesis of an appropriately oxygenated spiro compound related to the antitumor antibiotic fredericamycin A. *J. Org. Chem.* **1987**, *52*, 1339–1342.

(78) Bower, J. F.; Szeto, P.; Gallagher, T. Enantiopure 1,4-benzoxazines via 1,2-cyclic sulfamidates. Synthesis of levofloxacin. *Org. Lett.* **2007**, *9*, 3283–3286.

(79) Cacchi, S.; Ciattini, P. G.; Morera, E.; Ortar, G. Palladium-catalyzed triethylammonium formate reduction of aryl triflates. A selective method for the deoxygenation of phenols. *Tetrahedron Lett.* **1986**, *27*, 5541–5544.

(80) Chen, Q.-Y.; He, Y.-B.; Yang, Z.-Y. A new method for reduction of phenyl fluoroalkanesulphonates to arenes catalysed by palladium. *J. Chem. Soc., Chem. Commun.* **1986**, 1452–1453.

(81) Cabri, W.; De Bernardinis, S.; Francalanci, F.; Penco, S.; Santi, R. Palladium-catalyzed reduction of aryl sulfonates. Reduction versus hydrolysis selectivity control. *J. Org. Chem.* **1990**, *55*, 350–353.

(82) Kotsuki, H.; Datta, P. K.; Hayakawa, H.; Suenaga, H. An efficient procedure for palladium-catalyzed reduction of aryl/enol triflates. *Synthesis* **1995**, 1348–1350.

(83) Olah, G. A.; Ohannesian, L.; Arvanaghi, M. Synthetic methods and reactions. 119. N-Formylmorpholine: a new and effective formylating agent for the preparation of aldehydes and dialkyl (1-formylalkyl)phosphonates from Grignard or organolithium reagents. *J. Org. Chem.* **1984**, *49*, 3856–3857.

(84) Iritani, K.; Matsubara, S.; Utimoto, K. Palladium catalyzed reaction of 2-alkynylanilines with allyl chlorides. Formation of 3-allylindoles. *Tetrahedron Lett.* **1988**, *29*, 1799–1802.

(85) Kursanov, D. N.; Parnes, Z. N.; Loim, N. M. Applications of ionic hydrogenation to organic synthesis. *Synthesis* **1974**, 633–651.

(86) Lanzilotti, A. E.; Littell, R.; Fanshawe, W. J.; McKenzie, T. C.; Lovell, F. M. Stereoselective reduction of some indoles with triethylsilane-trifluoroacetic acid. *J. Org. Chem.* **1979**, *44*, 4809–4813.

(87) Boechat, N.; Clark, J. H. Fluorodenitrations using tetramethylammonium fluoride. *J. Chem. Soc., Chem. Commun.* **1993**, 921–922.

(88) Schimler, S. D.; Ryan, S. J.; Bland, D. C.; Anderson, J. E.; Sanford, M. S. Anhydrous tetramethylammonium fluoride for room-temperature SNAr fluorination. *J. Org. Chem.* **2015**, *80*, 12137–12145.

(89) Doyle, M. P.; Bryker, W. J. Alkyl nitrite-metal halide deamination reactions. 6. Direct synthesis of arenediazonium tetrafluoroborate salts from aromatic amines, tert-butyl nitrite, and boron trifluoride etherate in anhydrous media. *J. Org. Chem.* **1979**, *44*, 1572–1574.

(90) Wassmundt, F. W.; Kiesman, W. F. Efficient catalysis of hydrodediazoniations in dimethylformamide. *J. Org. Chem.* **1995**, *60*, 1713–1719.

(91) Hosomi, A.; Sakata, Y.; Sakurai, H. N-(trimethylsilylmethyl)-aminomethyl ethers as azomethine ylide synthons. A new and convenient access to pyrrolidine derivatives. *Chem. Lett.* **1984**, *13*, 1117–1120.

(92) Terao, Y.; Kotaki, H.; Imai, N.; Achiwa, K. Trifluoroacetic acid-catalyzed 1,3-cycloaddition of the simplest iminium ylide leading to 3- or 3,4-substituted pyrrolidines and 2,5-dihydropyrroles. *Chem. Pharm. Bull.* **1985**, *33*, 2762–2766.

(93) Kozmin, S. A.; Rawal, V. H. Preparation and Diels–Alder Reactivity of 1-Amino-3-siloxy-1,3-butadienes. *J. Org. Chem.* **1997**, *62*, 5252–5253.

(94) Kozmin, S. A.; Janey, J. M.; Rawal, V. H. 1-Amino-3-siloxy-1,3-butadienes: Highly Reactive Dienes for the Diels–Alder Reaction. *J. Org. Chem.* **1999**, *64*, 3039–3052.

(95) Chen, Q.; Wu, S. Perfluoro- and polyfluorosulfonic acids. 21. Synthesis of difluoromethyl esters using fluorosulfonyldifluoroacetic acid as a difluorocarbene precursor. *J. Org. Chem.* **1989**, *54*, 3023–3027.

(96) Chen, Q.-Y.; Wu, S.-W. A simple convenient method for preparation of difluoromethyl ethers using fluorosulfonyldifluoroacetic acid as a difluorocarbene precursor. *J. Fluorine Chem.* **1989**, *44*, 433–440.

(97) Clinical Laboratory Standards Institute (CLSI). *Methods for Dilution Antimicrobial Susceptibility Tests for Bacteria That Grow Aerobically*, 11th ed.; Clinical and Laboratory Standards Institute, 2018.

(98) McCoy, A. J.; Grosse-Kunstleve, R. W.; Adams, P. D.; Winn, M. D.; Storoni, L. C.; Read, R. J. Phaser crystallographic software. *J. Appl. Crystallogr.* **2007**, *40*, 658–674.

(99) Emsley, P.; Cowtan, K. Coot: model-building tools for molecular graphics. *Acta Crystallogr., Sect. D: Struct. Biol.* **2004**, *60*, 2126–2132.

(100) Emsley, P.; Lohkamp, B.; Scott, W. G.; Cowtan, K. Features and development of Coot. *Acta Crystallogr., Sect. D: Struct. Biol.* **2010**, *66*, 486–501.

(101) Adams, P. D.; Afonine, P. V.; Bunkóczi, G.; Chen, V. B.; Davis, I. W.; Echols, N.; Headd, J. J.; Hung, L.-W.; Kapral, G. J.; Grosse-Kunstleve, R. W.; McCoy, A. J.; Moriarty, N. W.; Oeffner, R.; Read, R. J.; Richardson, D. C.; Richardson, J. S.; Terwilliger, T. C.; Zwart, P. H. PHENIX: a comprehensive Python-based system for macromolecular structure solution. *Acta Crystallogr., Sect. D: Struct. Biol.* **2010**, *66*, 213–221.

(102) Liebschner, D.; Afonine, P. V.; Baker, M. L.; Bunkóczi, G.; Chen, V. B.; Croll, T. I.; Hintze, B.; Hung, L.-W.; Jain, S.; McCoy, A. J.; Moriarty, N. W.; Oeffner, R. D.; Poon, B. K.; Prisant, M. G.; Read, R. J.; Richardson, J. S.; Richardson, D. C.; Sammito, M. D.; Sobolev, O. V.; Stockwell, D. H.; Terwilliger, T. C.; Urzhumtsev, A. G.; Videau, L. L.; Williams, C. J.; Adams, P. D. Macromolecular structure determination using X-rays, neutrons and electrons: recent developments in Phenix. *Acta Crystallogr., Sect. D: Struct. Biol.* **2019**, *75*, 861–877.

(103) Van Der Sluis, P.; Spek, A. L. BYPASS: an effective method for the refinement of crystal structures containing disordered solvent regions. *Acta Crystallogr., Sect. A: Found. Crystallogr.* **1990**, *46*, 194–201.

(104) Gedeck, P.; Lu, Y.; Skolnik, S.; Rodde, S.; Dollinger, G.; Jia, W.; Berellini, G.; Vianello, R.; Faller, B.; Lombardo, F. Benefit of retraining pKa models studied using internally measured data. *J. Chem. Inf. Model.* **2015**, *55*, 1449–1459.

(105) Allen, R. I.; Box, K. J.; Comer, J. E. A.; Peake, C.; Tam, K. Y. Multiwavelength spectrophotometric determination of acid dissociation constants of ionizable drugs. *J. Pharm. Biomed. Anal.* **1998**, *17*, 699–712.

(106) Takács-Novák, K.; Box, K. J.; Avdeef, A. Potentiometric pKa determination of water-insoluble compounds: validation study in methanol/water mixtures. *Int. J. Pharm.* **1997**, *151*, 235–248.

(107) Avdeef, A. pH-Metric log P. Part 1. Difference Plots for Determining Ion-Pair Octanol-Water Partition Coefficients of Multiprotic Substances. *Quant. Struct.-Act. Relat.* **1992**, *11*, 510–517.

(108) Avdeef, A. pH-metric log P. Part 2. Refinement of partition coefficients and ionization constants of multiprotic substances. *J. Pharm. Sci.* **1993**, *82*, 183–190.

(109) Cao, X.; Lee, Y. T.; Holmqvist, M.; Lin, Y.; Ni, Y.; Mikhailov, D.; Zhang, H.; Hogan, C.; Zhou, L.; Lu, Q.; Digan, M. E.; Urban, L.; Erdemli, G. Cardiac ion channel safety profiling on the IonWorks Quattro automated patch clamp system. *Assay Drug Dev. Technol.* **2010**, *8*, 766–780.